Atmos. Chem. Phys., 8, 5731–5754, 2008
www.atmos-chem-phys.net/8/5731/2008/

Atmospheric Chemistry and Physics

Odin stratospheric proxy NO_y measurements and climatology

S. Brohede[1], C. A. McLinden[2], J. Urban[1], C. S. Haley[3], A. I. Jonsson[4], and D. Murtagh[1]

[1]Department of Radio and Space Science, Chalmers University of Technology, 412 96 Göteborg, Sweden
[2]Environment Canada, 4905 Dufferin Street, Toronto, Ontario, M3H 5T4, Canada
[3]Centre for Research in Earth and Space Science, York University, 4700 Keele Street, Toronto, Ontario, M3J 1P3, Canada
[4]Department of Physics, University of Toronto, M5S 1A7 Toronto, Ontario, Canada

Received: 3 January 2008 – Published in Atmos. Chem. Phys. Discuss.: 19 March 2008
Revised: 12 June 2008 – Accepted: 20 August 2008 – Published: 1 October 2008

Abstract. Five years of OSIRIS (Optical Spectrograph and InfraRed Imager System) NO_2 and SMR (Sub-millimetre and Millimetre Radiometer) HNO_3 observations from the Odin satellite, combined with data from a photochemical box model, have been used to construct a stratospheric proxy NO_y data set including the gases: NO, NO_2, HNO_3, $2\times N_2O_5$ and $ClONO_2$. This Odin NO_y climatology is based on all daytime measurements and contains monthly mean and standard deviation, expressed as mixing ratio or number density, as function of latitude or equivalent latitude (5° bins) on 17 vertical layers (altitude, pressure or potential temperature) between 14 and 46 km. Comparisons with coincident NO_y profiles from the Atmospheric Chemistry Experiment-Fourier Transform Spectrometer (ACE-FTS) instrument were used to evaluate several methods to combine Odin observations with model data. This comparison indicates that the most appropriate merging technique uses OSIRIS measurements of NO_2, scaled with model NO/NO_2 ratios, to estimate NO. The sum of $2\times N_2O_5$ and $ClONO_2$ is estimated from uncertainty-based weighted averages of scaled observations of SMR HNO_3 and OSIRIS NO_2. Comparisons with ACE-FTS suggest the precision (random error) and accuracy (systematic error) of Odin NO_y profiles are about 15% and 20%, respectively. Further comparisons between Odin and the Canadian Middle Atmosphere Model (CMAM) show agreement to within 20% and 2 ppb throughout most of the stratosphere except in the polar vortices. The combination of good temporal and spatial coverage, a relatively long data record, and good accuracy and precision make this a valuable NO_y product for various atmospheric studies and model assessments.

Correspondence to: S. Brohede
(samuel.brohede@chalmers.se)

1 Introduction

Reactive nitrogen species, known collectively as NO_y (where NO_y is the sum of NO, NO_2, NO_3, HNO_3, $2\times N_2O_5$, $ClONO_2$, $BrONO_2$ and HO_2NO_2), play an important role in stratospheric ozone chemistry and are intimately linked to hydrogen, chlorine, and bromine compounds. Reactive nitrogen species are the largest contributors to ozone destruction in the middle stratosphere, primarily via catalytic cycles involving NO and NO_2 (collectively known as NO_x). In the lower stratosphere NO_y also indirectly influences ozone through its influence on the partitioning of the hydrogen, chlorine, and bromine families.

The primary source of stratospheric NO_y is the oxidation of N_2O; that is,

$$N_2O+O(^1D)\rightarrow NO+NO \quad \text{(R1)}$$

where $O(^1D)$ is an exited state of atomic oxygen, mainly produced from O_3 photolysis. The source of N_2O is a combination of natural and anthropogenic surface sources. Due mainly to its use in agriculture, N_2O is increasing at a rate of 2.6%/decade (Forster et al., 2007). A much smaller, and more sporadic source, is downward transport from the mesosphere of NO created by the precipitation of energetic particles in the polar regions (Randall et al., 2005; Funke et al., 2005a; Randall et al., 2007; Seppälä et al., 2007). This source represents about 2% of total stratospheric NO_y (Vitt et al., 2000). More recently, Funke et al. (2005a) have found that the NO_x transported into the stratosphere during Antarctic polar winter may represent up to 9% of total stratospheric NO_y in the Southern Hemisphere. The loss of stratospheric NO_y occurs via transport into the troposphere, and through the reaction sequence

$$NO+h\nu\rightarrow N+O \quad \text{(R2)}$$

Published by Copernicus Publications on behalf of the European Geosciences Union.

$$N+NO \rightarrow N_2+O \quad (R3)$$

and so is quadratic in NO_y. Photolysis of NO only occurs above ∼40 km. The photochemical life time of NO_y with respect to Reaction (R3) ranges from decades in the lower stratosphere to months near the stratopause (Nevison et al., 1997) i.e. much longer than or comparable to typical transport time scales. Thus in the lower stratosphere NO_y is controlled primarily by transport processes. Photo-chemistry gains increasing influence on the NO_y abundance with increasing altitude.

During polar night and spring, NO_y can be removed from the gas phase by sequestering HNO_3 in Polar Stratospheric Cloud (PSC) particles, through heterogeneous chemistry. Sedimentation of PSC particles can lead to a permanent removal of NO_y from the polar lower stratosphere, often referred to as denitrification. As particles evaporate at lower altitudes, enhancements of NO_y have been observed (Kleinböhl et al., 2005; Dibb et al., 2006), denoted re-nitrification.

The trend in N_2O is expected to lead to an upward trend in NO_y. However, due to insufficient observations, such a trend has not been verified directly. McLinden et al. (2001) suggested that the rate of increase in NO_y should be about three-quarters that of N_2O due to simultaneous trends in stratospheric ozone and temperature. An increase in column-NO_2 at >5%/decade has been reported (Liley et al., 2000), which is consistent with an increase in NO_y combined with a shift in the NO_2/NO_y partitioning due to changes in ozone, temperature, halogens, and possibly aerosol loading over the length of the time series (Fish et al., 2000; McLinden et al., 2001).

Many models have been used to simulate NO_y abundances in the stratosphere. The Models and Measurements Intercomparison II (Brasseur and Remsberg, 1999, Sects. 3.3.6 and 3.5.1), which compared NO_y from 13 two-dimensional and three-dimensional models, revealed a spread in excess of 30% when the N_2O source was constrained. Much of this inter-model difference was attributed to model dynamics. Differences between the models and the UARS (Upper Atmosphere Research Satellite) observations of (pseudo-)NO_y were considerably larger. The latest generation of models appear to be more capable of simulating global stratospheric NO_y. For example, the ECHAM5/MESSy1 (European Centre Hamburg Model 5/Modular Earth Submodel System 1) chemistry-climate model with nudged meteorology revealed good agreement with MIPAS (Michelson Interferometer for Passive Atmospheric Sounding) NO_y (Brühl et al., 2007) over a three-day period in 2002. In general, however, there is a lack of global, long term NO_y observations to evaluate these models. Other types of photochemical models must be initialized with an NO_y profile or field that is generally based on output from a 3-D model, a correlation with N_2O, or both. Here too, the lack of global NO_y observations are noticeable.

With the exception of the lower stratosphere, measurements of stratospheric NO_y must be done remotely. In general, estimation of NO_y requires a measurement of all major NO_y species. This includes the "big five" (i.e. NO, NO_2, HNO_3, $2\times N_2O_5$ and $ClONO_2$) which collectively comprise 96–99% of NO_y during daytime, according to box model calculations (Fig. 1). At specific altitudes or local times, one or more of these species may be neglected without compromising the result; for example, stratospheric NO at night. However, instruments generally measure only a subset of the required species and therefore only an estimate of NO_y is obtained. LIMS (Limb Infrared Monitor of the Stratosphere), 1978–1979 (Gille and Russel, 1984), was the first satellite instrument to estimate NO_y by measuring HNO_3 and NO_2 at night. Measurements of HALOE (Halogen Occultation Experiment) NO and NO_2 with CLAES (Cryogenic Limb Array Etalon Spectrometer) HNO_3 and $ClONO_2$, both on UARS, have been merged to create a pseudo-NO_y climatology (Danilin et al., 1999), however perturbed by the major volcanic eruption of Mt. Pinatubo (1991). The first instrument to measure all five major species was ATMOS (Atmospheric Trace gas Molecule Spectroscopy) (Russell et al., 1988) over four deployments from the space shuttle. Envisat/MIPAS was the first satellite instrument to measure all major NO_y species (Mengistu Tsidu et al., 2005; Fischer et al., 2008), but with complete data available only between July 2002 and March 2004 and sporadic thereafter. In addition, the MIPAS NO and NO_2 retrievals require complicated non-LTE (Local Thermodynamic Equilibrium) calculations (Funke et al., 2005b). More recently, the ACE-FTS (Atmospheric Chemistry Experiment-Fourier Transform Spectrometer) (Bernath et al., 2005) launched in 2004, a satellite successor to ATMOS, is able to measure all primary species. While ACE-FTS has collected more than four years of data, its sparse coverage (2 profiles per orbit) means that global coverage is achieved only over several months.

Complementary to the MIPAS and ACE-FTS instruments is the Odin satellite. Odin observes NO_2 profiles with the Optical Spectrograph and Infra-Red Imager System (OSIRIS) and HNO_3 with the Sub-millimetre and Millimetre Radiometer (SMR) in the stratosphere, see Sect. 2.1. In total, Odin measures about 75% of total NO_y at 20 km but only 25% at 40 km (see Fig. 1). Hence, a simple addition of OSIRIS NO_2 and SMR HNO_3 will be of limited use. In this study we investigate the construction of a "proxy" NO_y data set by combining Odin measurements with a photochemical box model, constrained with additional observations, to account for the missing species. This is, to our knowledge, the first description of such a proxy NO_y data set. The length of the Odin data set of more than seven years, combined with good spatial coverage provides a valuable NO_y product, complementary to that of MIPAS, ACE-FTS, and preceding missions.

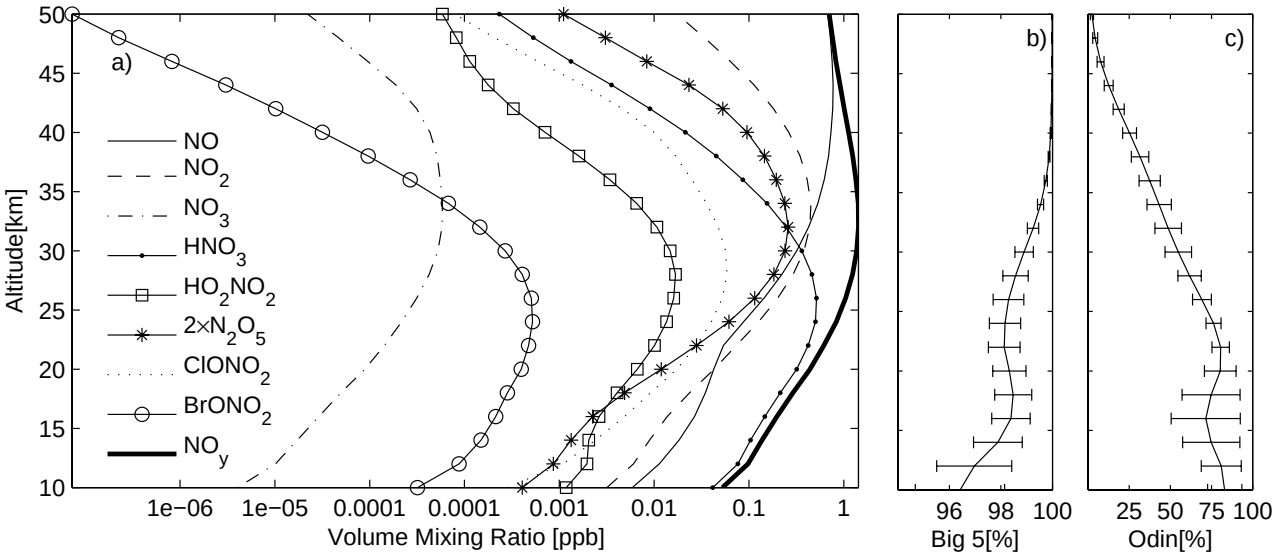

Fig. 1. NO_y partitioning and total NO_y (thick solid line) given by the University of California, Irvine, photochemical box model. The profiles correspond to average concentrations for simulations given at all OSIRIS measurement locations (both a.m. and p.m.) from 2002 to 2006 **(a)**. Panel **(b)** gives the ratio of the big five ($NO+NO_2+HNO_3+2\times N_2O_5+ClONO_2$) to the total NO_y expressed as mean (line) and 1σ standard deviation (error bars). Panel **(c)** shows the ratio of the Odin NO_y species (NO_2+HNO_3) to the concentration of the big five expressed as mean (line).

Section 2 gives a brief overview of the Odin instruments and other data sets used in this study. This is followed by a detailed description on the construction of the Odin proxy NO_y data set (Sect. 3). Results are discussed in Sect. 4 which includes a comparison with the Canadian Middle Atmosphere Model (CMAM). This is followed by a summary of the major conclusions in Sect. 6.

2 Data sources

Information on the various data sets used in this study is provided below.

2.1 Odin observations

The Odin satellite was launched in February 2001 into a 600 km circular sun-synchronous near-terminator orbit with a 97.8° inclination and an equator crossing time of the ascending node at 18:00 local solar time (LST) (Murtagh et al., 2002). Odin carries two instruments: OSIRIS (Llewellyn et al., 2004) and SMR (Frisk et al., 2003). The instruments are co-aligned and scan the limb of the atmosphere over a tangent height range from 7 km to 70 km in approximately 85 s during normal stratospheric operations through controlled nodding of the satellite. With 14–15 orbits per day and 40–60 limb scans on the day-side per orbit, about 600 day-side profiles are obtained per day. Due to Odin's orbit, the data from both instruments are generally limited to between 82° N and 82° S. The LST is close to 18:00 and 06:00 for low and mid latitudes during the ascending and descending nodes, respectively, but sweeps quickly over local midnight and noon at the poles. The equator crossing time is slowly drifting later in LST during the Odin mission. Since OSIRIS is dependent on sunlight, the full latitude range is only covered around the equinoxes and hemispheric coverage is provided elsewhere.

The SMR instrument measures thermal emissions and comprises five receivers, one millimeter receiver at 118 GHz and four sub-millimeter receivers between 486–580 GHz (Murtagh et al., 2002; Frisk et al., 2003). The millimeter receiver is used for the observation of oxygen, which is mainly used for astronomical studies while the sub-millimeter receivers are used for the retrieval of several atmospheric species, including stratospheric ozone, HNO_3, ClO and N_2O. HNO_3 profiles are retrieved in a band centered at 544.6 GHz using a maximum a posteriori (MAP) inversion technique (Urban et al., 2006, 2007). Comparisons with measurements of other space-borne sensors such as MIPAS on the Envisat satellite and the Microwave Limb Sounder (MLS) on Aura indicate a positive bias of the order of 2 ppb around the vmr profile peak (∼23 km) and a small negative bias of roughly 0.5 ppb at 35–45 km (Urban et al., 2006; Santee et al., 2007; Wang et al., 2007a,b) as well as a possible altitude shift towards lower altitudes of approximately 1–2 km (Wang et al., 2007b). This work is based on the Chalmers version 2.0 of the HNO_3 data, using only profiles with good quality (assigned quality flag: QUALITY=0 or 4).

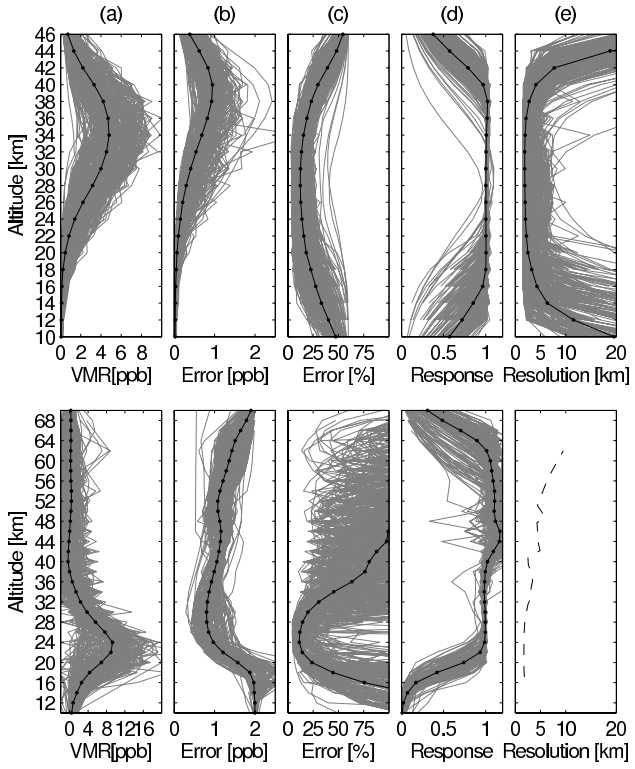

Fig. 2. Average characteristics of the Odin data sets. Upper panel is showing OSIRIS NO_2 characteristics and the lower SMR HNO_3. **(a)** median mixing ratio profile (black line) and an ensemble of profiles (gray lines), **(b)** median absolute retrieval error (black line) and an ensemble of error profiles (gray lines), **(c)** median relative retrieval error (black line) and an ensemble of error profiles (gray lines), **(d)** median measurement response (black line) and an ensemble of measurement response profiles (gray lines), **(e)** median altitude resolution (spread of the averaging kernels) (black line) and an ensemble of resolution profiles (gray lines). The medians are based on Odin data from every tenth orbit (January 2002 to December 2006) and the ensemble profiles correspond to every thousandth measurement. No information on the individual profile altitude resolution is given in the SMR data set, but a typical estimate from (Urban et al., 2007) is plotted (dashed line). Note that the SMR and OSIRIS altitude scales are not identical.

OSIRIS contains two optically independent components, the Optical Spectrograph (OS) and the InfraRed Imager (IRI). The OS is a grating spectrometer that measures limb-scattered sunlight spectra in the spectral range from 280 nm to 800 nm at a resolution of about 1 nm. The IRI is a three channel camera, imaging the atmospheric airglow emissions near 1.27 μm and 1.53 μm in a limb-viewing tomographic mode (Degenstein et al., 2002). The OS scattered sunlight measurements are used to provide vertical profiles of minor stratospheric constituents including O_3 (von Savigny et al., 2003; Haley and Brohede, 2007), NO_2 (Haley et al., 2004), OClO (Krecl et al., 2006) and aerosol (Bourassa et al., 2007). The official OSIRIS NO_2 product, used in this study, is retrieved using a combination of differential optical absorption spectroscopy (DOAS) (Platt, 1994) and MAP using wavelengths between 435 and 451 nm. The most recently updated version (3.0) is estimated to have random and systematic uncertainties in the middle stratosphere of 6% and 10–20%, respectively, based on intercomparions with various solar occultation instruments (Brohede et al., 2007a; Haley and Brohede, 2007). Additionally, OSIRIS climatological NO_2 is found to be consistent with the REPROBUS Chemical Transport Model (CTM) (Lefèvre et al., 1994, 1998) to within 20% throughout the stratosphere and all latitudes and seasons, except in the polar vortex region and in the tropical upper troposphere/lower stratosphere (Brohede et al., 2007c). This work uses the version 3.0 of the NO_2 data where profiles, flagged for possible inaccurate pointing, are excluded.

The vertical resolution of OSIRIS NO_2 and SMR HNO_3 is about 2 km in the middle stratosphere and a high measurement responses (>0.5) is usually found between 15 and 42 km for NO_2 and between 20 and 66 km for HNO_3, but is profile dependent. The retrieval errors (measurement noise + smoothing error) at the profile peaks are around 15% ($\sim$1 ppb) for NO_2 and 12% ($\sim$1 ppb) for HNO_3, but increase rapidly at higher and lower altitudes for HNO_3, see Fig. 2. Note that both data sets are based on similar inversion methods, although NO_2 profiles are retrieved in log-space and HNO_3 in linear space. SMR and OSIRIS stratospheric ozone products are found to be very consistent, providing confidence in the robustness and long-term stability of the fundamentally different measurement techniques (Brohede et al., 2007b).

2.2 ACE-FTS observations

The Fourier Transform Spectrometer (FTS) is the primary instrument onboard the Atmospheric Chemistry Experiment (ACE) satellite (also known as SCISAT-1). The satellite was launched in August 2003 into a 650 km altitude and 74° inclination orbit and is operating in solar occultation mode. The ACE-FTS instrument is a high resolution (0.02 cm^{-1}) spectrometer operating from 2.2 to 13.3 μm (Bernath et al., 2005). ACE-FTS provides mixing ratio profiles with around 4 km altitude resolution for various atmospheric compounds including the following NO_y species (with typical altitude range in brackets): NO (15–110 km), NO_2 (13–57 km), HNO_3 (5–37 km), $ClONO_2$ (13–35 km), and N_2O_5 (15–39 km). This makes a common range for all the big five NO_y species ($NO+NO_2+HNO_3+2\times N_2O_5+ClONO_2$) of 15–35 km. According to the recent validation study by Wolff et al. (2008), HNO_3 agrees with MIPAS and MLS to within 10% between 10 and 36 km and $ClONO_2$ and N_2O_5 (daytime) agrees with MIPAS between 16 and 27 km to 0.01 ppb and 0.02 ppb, respectively. Furthermore, NO_2 agrees with a range of various instruments to within 20% between 25 and 40 km, with a possible ACE-FTS negative bias of around

10% and NO is found to agree with HALOE to better than 8% between 22 and 64 km (Kerzenmacher et al., 2008). Additionally, a study of the NO_y budget has been conducted using the ACE-FTS data (Qin, 2007). For this study we have used data version 2.2 (version 2.2-update for N_2O_5), excluding any ACE occultations flagged for potential retrieval problems. ACE-FTS also measures the next most abundant NO_y species, HO_2NO_2, but only over a limited altitude range.

2.3 The photochemical box model

Since only Odin data are used, information on the missing key NO_y species (NO, N_2O_5, and $ClONO_2$) is supplied by a photochemical model. In this work the University of California, Irvine, photochemical box model (Prather, 1992; McLinden et al., 2000) is employed to calculate the local NO_y partitioning. For a particular simulation, profiles for the background atmosphere (pressure and temperature), ozone, long-lived tracers (N_2O, H_2O, CH_4), and the families (NO_y, Cl_y, and Br_y) need to be specified. All remaining species are calculated to be in a 24-h steady-state by integrating the model for 30 days (but fixed to a given Julian day). The model is run with 25 pressure-altitude levels between 10 and 58 km, but all interpolations are done using true altitudes. Heterogeneous chemistry on background stratospheric aerosols is prescribed by the model, but no PSCs are included.

Pressure and temperature are obtained from the European Centre for Medium-Range Weather Forcasts (ECMWF) reanalysis and the ozone profile is measured simultaneously by OSIRIS (Roth et al., 2007). Of the remaining fields, N_2O and NO_y are monthly-means from a three-dimensional chemical transport model (Olsen et al., 2001) and Cl_y and Br_y are from tracer correlations with N_2O (R. Salawitch, personal communication, 2003). Note that the NO_y partitioning is largely independent on the total NO_y as discussed further in Sect. 3.1. Surface albedo is taken from the Global Ozone Monitoring Experiment (GOME) monthly-mean clear-sky surface reflectivity climatology at 416 nm (Koelemeijer et al., 2003). When a cloud is detected at the bottom of the limb scan, the albedo is taken as the mean of the clear sky albedo and 0.6 since no information on cloud thickness and brightness is available. Using this methodology, a simulation has been performed for each Odin limb scan. Results from an evaluation of the ability of the box model to calculate the NO_y partitioning, as determined through comparisons with the JPL MkIV interferometer, are presented in Appendix A. Further information on this model accompanied with a sensitivity study is found in Appendix A of Brohede et al. (2007c).

2.4 CMAM simulations

The Canadian Middle Atmosphere Model (CMAM) is a three-dimensional coupled chemistry-climate model (CCM) with comprehensive physical parameterization (Beagley et al., 1997; de Grandpré et al., 2000). The model version used here has a vertical domain from the Earth's surface to approximately 97 km. It has 71 vertical levels (approximately 3 km vertical resolution in the middle atmosphere) and T31 spectral horizontal resolution (corresponding to roughly 6° latitude/longitude grid spacing).

The model includes interactive stratospheric chemistry with all the relevant catalytic ozone loss cycles and heterogeneous reactions on sulphate aerosols and PSCs. The model includes parameterizations for Type 1b PSCs (super-cooled ternary solutions) and Type 2 PSCs (water ice). There is no parameterization for Type 1a PSCs (nitric acid trihydrate particles) and sedimentation of particles is not implemented. Thus the model does not simulate permanent removal of NO_y through denitrification via the sedimentation of PSC particles in the stratospheric winter polar vortices. In addition, a numerical problem related to the PSCs in the model was identified during the course of this work, leading to highly overestimated NO_y values in the southern polar lower stratosphere during spring. Work is being undertaken to address this problem, but for this study the region in question, i.e. southward of 50° S and below 10 hPa during September to January is masked out. Other regions in the model are not affected.

CMAM data from an ensemble of transient simulations in which the model was forced by observed surface values of CO_2, CH_4, N_2O and halogens in the past, and by a scenario in the future (following the SPARC CCMVal REF2 specifications described by Eyring et al., 2005) are used here. Each ensemble member used a different set of inter-annually varying sea-surface temperature realizations from a coupled atmosphere-ocean model. A basic evaluation of CMAM and comparison with observations and other models is given in Eyring et al. (2007). The NO_y dataset used here represents the ensemble mean field averaged over the period 1996–2005. Note that CMAM employs the standard definition of NO_y ($NO+NO_2+NO_3+HNO_3+2\times N_2O_5+HO_2NO_2+ClONO_2$ $+BrONO_2$).

3 Method

This section describes the merging of the Odin data sets and the construction of the Odin proxy NO_y climatology. The data is referred to as "proxy" due to the intrinsic dependence on the photochemical box model to account for the missing species. An overview of the method is found in Fig. 3.

3.1 Data merging

It is not immediately clear how best to combine the Odin data with the model simulations. Simply adding the remaining NO_y species from the model would make the result critically dependent on the assumed NO_y profile in the box model and moreover would ignore any information contained in the

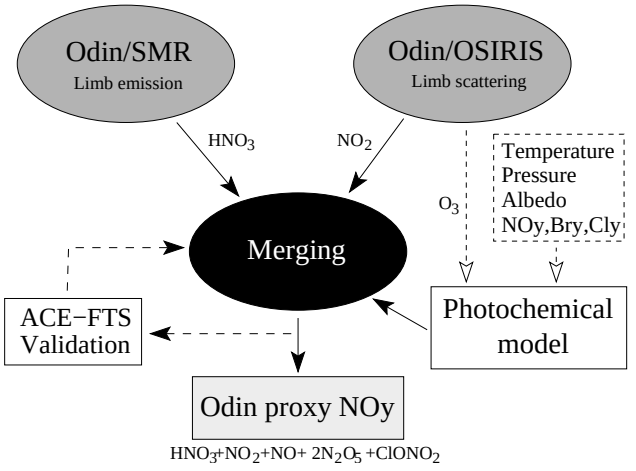

Fig. 3. Sketch of the method to construct the Odin proxy NO_y. OSIRIS NO_2 and SMR HNO_3 are merged by using a photochemical box model to compensate for the missing species (NO, $ClONO_2$ and N_2O_5). ACE-FTS observations are used to evaluate the merging theory and to estimate uncertainties. The photochemical box model is fed by local OSIRIS O_3, temperature and pressure from ECMWF, albedo from the GOME monthly-mean climatology (Koelemeijer et al., 2003), NO_y from a three-dimensional chemical transport model (Olsen et al., 2001) and Cl_y and Br_y from tracer correlations with N_2O.

Odin data due to the close coupling among the NO_y species. Thus it seems far better to rely on the model only for ratios or partitioning, as opposed to absolute abundances. Additionally, the NO_y partitioning is almost completely independent of the model NO_y over a wide range as explored in Sect. 3.4 and illustrated in Fig. 4.

3.1.1 Merging theory a

The most important of the missing NO_y species is NO which is very closely coupled to NO_2 through the reaction pair;

$$NO+O_3 \rightarrow NO_2+O_2 \quad \text{(R4)}$$

$$NO_2+h\nu \rightarrow NO+O. \quad \text{(R5)}$$

The lifetime of NO_2 against photolysis is of the order of 100 s in the middle stratosphere and so can be considered to be in photochemical equilibrium at daytime conditions. Secondary reactions that control the partitioning of NO_x include

$$NO_2+O \rightarrow NO+O_2 \quad \text{(R6)}$$

$$NO+HO_2 \rightarrow NO_2+OH \quad \text{(R7)}$$

$$NO+ClO \rightarrow NO_2+Cl \quad \text{(R8)}$$

$$NO+BrO \rightarrow NO_2+Br \quad \text{(R9)}$$

While Reactions R7–R9 may be important in the lower or middle stratosphere, Reactions R4–R6 tend to dominate over nearly the entire stratosphere and so to a good approximation the abundance of NO may be expressed as (de Grandpré et al., 1997);

$$[NO]=[NO_2]\frac{(J[NO_2]+k_1[O])}{k_2[O_3]}, \quad \text{(R10)}$$

where J is the photolysis rate of NO_2, Reaction (R5), k_1 is the reaction rate coefficient of Eq. (R6) and k_2 is the coefficient for Eq. (R4). This illustrates that with a good knowledge of NO_2, O_3, and temperature (required for the reaction rate coefficients), a reasonable representation of NO may be obtained. Thus NO is taken simply as the OSIRIS NO_2 scaled by the model calculated NO/NO_2 ratio (which would of course include the hydrogen, chlorine, and bromine reactions that impact the NO_x partitioning). As stated in section 2.3, the O_3 concentration comes from the corresponding OSIRIS measurement.

SMR HNO_3 is corrected for the systematic bias (see Sect. 2.1) prior to the merging by shifting the profiles upward by 1 km and applying a second order compensation function as found by ACE-FTS comparisons (see Fig. 5):

$$HNO_3^{SMR*}=1.11\cdot HNO_3^{SMR}-0.026(HNO_3^{SMR})^2, \quad (1)$$

where the concentration is expressed in ppb and * denotes a corrected concentration. Note that only a single correction function is derived which is based on the sparse (both temporally and spatially) ACE-FTS oservations and applied to Odin HNO_3 measurements at all latitudes, altitudes and seasons. As previously mentioned in Sect. 2.2, ACE-FTS agrees very well with both MIPAS and MLS (within 10% between 10–36 km) as found by Wolff et al. (2008). This justifies the idea of correcting SMR profiles rather than ACE-FTS and suggests that a similar adjustment to SMR-HNO_3 would be needed if using MIPAS or MLS data in the construction of the Odin proxy NO_y.

The remaining key NO_y species, N_2O_5 and $ClONO_2$, possess a lifetime between NO_2 and HNO_3 and are linked chemically to them and so both OSIRIS NO_2 and SMR HNO_3 are used with a weighting determined by their respective uncertainties. The resultant NO_y formulation is;

$$NO_y^{Odin}=NO_2^{OS}+HNO_3^{SMR*}+NO_2^{OS}\left(\frac{NO^{mod}}{NO_2^{mod}}\right)+NO_{rest}^{Odin} \quad (2)$$

$$NO_{rest}^{Odin}=\frac{1}{1/\sigma_{SMR}^2+1/\sigma_{OS}^2}\left(\frac{NO_{rest}^{SMR}}{\sigma_{SMR}^2}+\frac{NO_{rest}^{OS}}{\sigma_{OS}^2}\right) \quad (3)$$

$$NO_{rest}^{SMR}=HNO_3^{SMR*}\cdot\frac{2\times N_2O_5^{mod}+ClONO_2^{mod}}{HNO_3^{mod}} \quad (4)$$

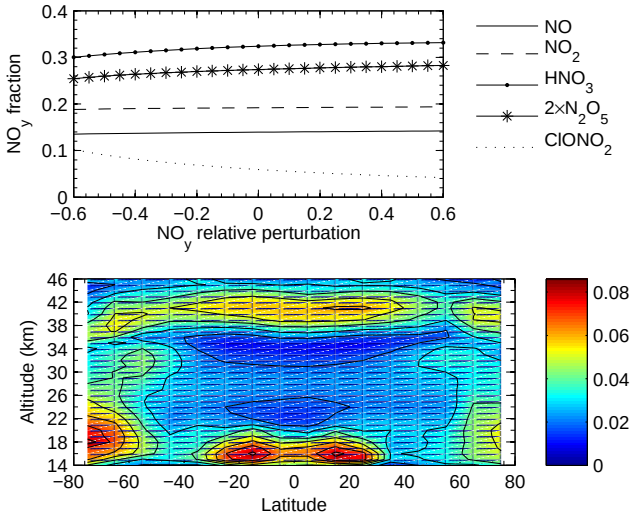

Fig. 4. Upper panel: Fraction of the five main NO_y species as computed in the photochemical box model as a function of the fraction of the perturbation of the total NO_y box model input, relative to the standard NO_y at 28 km, 45° N for 15 March. Lower panel: Maximum difference in NO_y fraction found in NO, NO_2, HNO_3 or $ClONO_2$+2×N_2O_5 due to a −0.6 and 0 and 0 and +0.6 perturbation of the total input NO_y. Note that the values presented correspond to the largest absolute differences found in any of the NO_y species, altitudes and months. Local solar times of the calculations simulate those of Odin's orbit on the descending (a.m.) node.

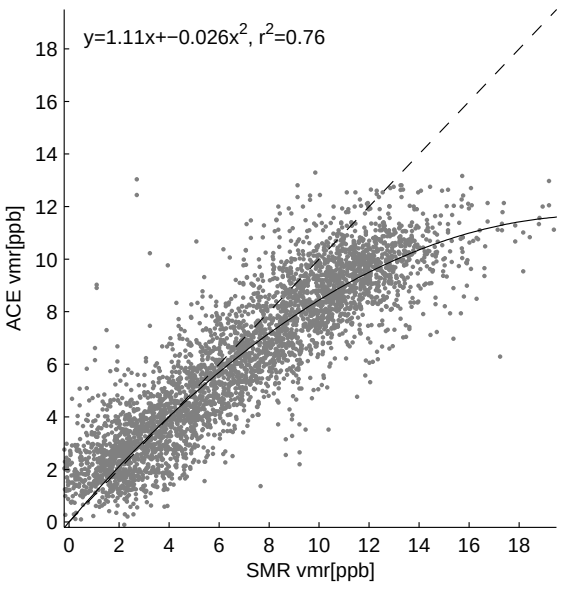

Fig. 5. Scatter plot of SMR versus ACE-FTS HNO_3 mixing ratios for all daylight coincident measurements 2002–2006 (grey dots). The systematic bias can be compensated for by a second order fit to the data (black line) with the corresponding equation (after applying a 1 km vertical shift of the SMR profiles).

$$NO^{OS}_{rest} = NO^{OS}_2 \cdot \frac{2 \times N_2O_5^{mod} + ClONO_2^{mod}}{NO_2^{mod}}, \quad (5)$$

where σ is the measurement uncertainty (smoothing error + measurement error), "mod" denotes modeled data as output from the photochemical box model, "OS" refers to OSIRIS and NO_{rest} is the sum of 2×N_2O_5 and $ClONO_2$. It makes sense that measurements of NO_2 are not used to estimate HNO_3 and vice versa.

As previously mentioned, the University of California, Irvine photochemical (stacked) box model (Prather, 1992; McLinden et al., 2000) is used here to calculate the partitioning. The box model is constrained by the local OSIRIS ozone (Roth et al., 2007) and the ECMWF temperature and pressure of the measurement. The scaling is done in mixing ratios, where OSIRIS number density profiles are converted using local temperature and pressure information from ECMWF.

While this theory (denoted *a*) is the most logical, additional candidates may be envisioned and it is worthwhile comparing them to the one described above. In total six additional formulations (*b* to *g*), outlined below, are assessed.

3.1.2 Merging theory b

This merging theory is based on the lifetime of the missing NO_y species with OSIRIS NO_2 used to scale up the short-lived NO and SMR HNO_3 for the longer lived $ClONO_2$. As N_2O_5 possesses an intermediate lifetime it is split equally between the two:

$$NO_y^{Odin} = HNO_3^{SMR*} \cdot \gamma_1 + NO_2^{OS} \cdot \gamma_2 \quad (6)$$

$$\gamma_1 = \frac{HNO_3^{mod} + ClONO_2^{mod} + N_2O_5^{mod}}{HNO_3^{mod}} \quad (7)$$

$$\gamma_2 = \frac{NO^{mod} + NO_2^{mod} + N_2O_5^{mod}}{NO_2^{mod}} \quad (8)$$

3.1.3 Merging theory c

Merging theory c is effectively a weighted average of total NO_y from both instruments using information on the specific measurement uncertainty of the individual data sets:

$$NO_y^{Odin} = \frac{1}{1/\sigma^2_{SMR} + 1/\sigma^2_{OS}} \left(\frac{NO_y^{SMR}}{\sigma^2_{SMR}} + \frac{NO_y^{OS}}{\sigma^2_{OS}} \right) \quad (9)$$

$$NO_y^{SMR} = HNO_3^{SMR*} \cdot \frac{NO_y^{mod}}{HNO_3^{mod}} \quad (10)$$

$$NO_y^{OS} = NO_2^{OS} \cdot \frac{NO_y^{mod}}{NO_2^{mod}}. \quad (11)$$

This method gives greatest weight to the data with the smallest uncertainty which usually is OSIRIS at high altitudes and SMR at the HNO_3 peak, see Fig. 2.

3.1.4 Merging theory d

This is the most straight forward way to merge the two data sets where the sum of OSIRIS NO_2 and SMR HNO_3 concentrations is scaled up to total NO_y:

$$NO_y^{Odin} = (HNO_3^{SMR*} + NO_2^{OS}) \cdot \gamma \quad (12)$$

$$\gamma = \frac{NO_y^{mod}}{NO_2^{mod} + HNO_3^{mod}} \quad (13)$$

3.1.5 Merging theory e

Here, OSIRIS NO_2 is used to estimate all the NO_y species except HNO_3 which is taken from the SMR measurements:

$$NO_y^{Odin} = HNO_3^{SMR*} + NO_2^{OS} \cdot \gamma \quad (14)$$

$$\gamma = \frac{2 \times N_2O_5^{mod} + ClONO_2^{mod} + NO^{mod} + NO_2^{mod}}{NO_2^{mod}} \quad (15)$$

This theory might be justified as the uncertainty of OSIRIS is usually lower than SMR and additionally does not possess a systematic bias.

3.1.6 Merging theory f

Here only SMR HNO_3 data are used to scale to total NO_y,

$$NO_y^{Odin} = HNO_3^{SMR*} \frac{NO_y^{mod}}{HNO_3^{mod}} \quad (16)$$

3.1.7 Merging theory g

Finally, for completeness, only OSIRIS NO_2 data are used to scale to total NO_y,

$$NO_y^{Odin} = NO_2^{OS} \frac{NO_y^{mod}}{NO_2^{mod}} \quad (17)$$

3.2 Evaluation of the merging theories

ACE-FTS solar occultation observations (see Sect. 2.2) of the big five NO_y species are used to evaluate the different merging theories. This is done by studying the statistical differences between ACE-FTS and Odin coincident profiles, found within 04:00 UT and 500 km of Odin measurements from 2003–2006. Occasions where one profile is inside the polar vortex and the other outside are discarded based on information on potential vorticity (PV) from ECMWF. The coincidences are divided into three latitude bands: southern latitudes ($90° S \leq lat < 30° S$), equatorial latitudes ($30° S \leq lat \leq 30° N$) and northern latitudes ($30° N < lat \leq 90° N$). This division limits the impact of different atmospheric conditions on the comparisons, including cloudiness and tropopause height. In addition, the data are divided into four seasons: November–December–January (N–D–J), February–March (F–M), April–May–June–July–August (A–M–J–J–A) and September–October (S–O). This division is logical when considering the OSIRIS latitude coverage over the year, where the Northern Hemisphere is covered between April and August, the Southern Hemisphere is covered from November to January and full global coverage is achieved only close to the equinoxes (S–O and F–M)

A statistical analysis is carried out when more than 10 coincidences are found within a latitude/season category (profiles and individual altitudes). Systematic differences are studied through the mean of the relative differences with respect to ACE:

$$\bar{\Delta}(z) = \frac{1}{n} \sum_{i=1}^{n} \left[\frac{Odin_i(z) - ACE_i(z)}{ACE_i(z)} \right], \quad (18)$$

where $Odin_i$ and ACE_i represent the Odin and ACE measurements of NO_y, respectively, n is the number of coincidences and z is the altitude. Random differences are studied using the standard deviation of the relative differences:

$$\sigma_\Delta(z) = \sqrt{\frac{1}{n-1} \sum_{i=1}^{n} \left[\left(\frac{Odin_i(z) - ACE_i(z)}{ACE_i(z)} \right) - \bar{\Delta}(z) \right]^2} \quad (19)$$

The results from the different latitude/season bins indicate anomalous features in F-M northern latitudes, which happen to coincide with the bin where most of the coincidences occur and is probably related to additional uncertainties in the proximity of Arctic polar vortex. Approximately 400 coincidences were found outside F-M northern latitudes and 340 within. Outside the F-M northern latitudes, all of the NO_y theories, except f and g agree to ACE-FTS within 1.25 ppb (or 20%) systematically and 50% (1σ) randomly above 20 km, see upper panel of Fig. 6. Evidently, using both Odin data sets to estimate NO_y is more accurate than using only one of them, however it is difficult to disentangle the skill of the different merging theories a to e. In the F-M northern latitude bin, the differences between the theories are more clear, see lower panel of Fig. 6. From these

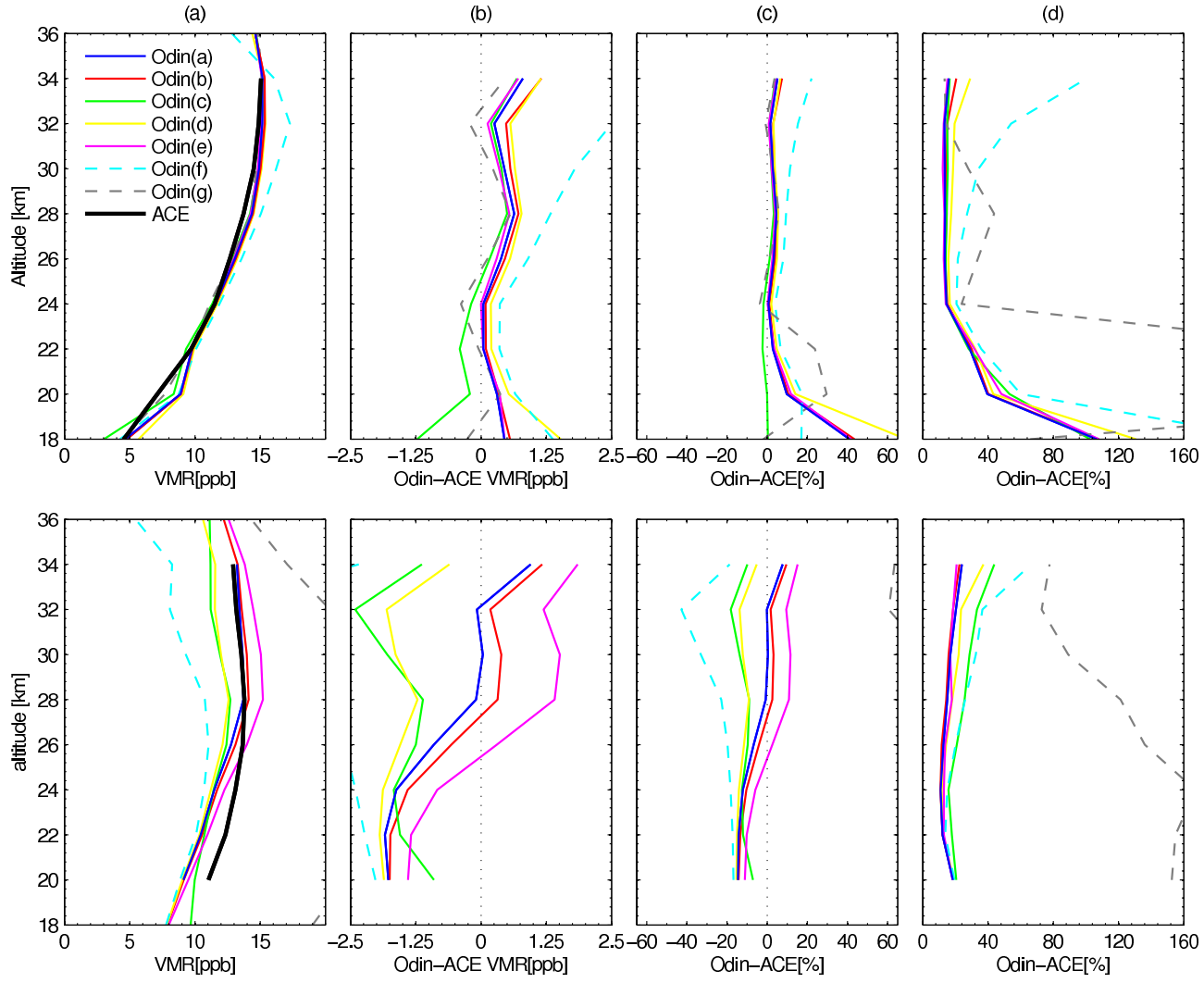

Fig. 6. Comparisons of the Odin proxy NO_y theories (see Sect. 3.1) and ACE-FTS observations of the total (big five) NO_y species for all latitudes and seasons, excluding northern latitudes in February and March, (upper panel) and only northern latitudes in February and March (lower panel). Column **(a)** shows the mean mixing ratio profiles, **(b)** the mean of the absolute individual differences (Odin-ACE), **(c)** the mean of the relative individual differences (Odin-ACE)/ACE and **(d)** the 1σ relative standard deviation of the individual differences.

coincidences, it is concluded that theory *a* or *b* show the smallest systematic and random difference over the entire altitude range as compared to ACE-FTS observations. Note that theory *g* produces largest differences in this bin, probably due to a combination of enhanced measurement uncertainties and difficulties in NO_y partitioning of the box model.

Less extreme outliers in theory *a* than *b* in some of the latitude/season bins (not shown) further justify choosing this theory for constructing the Odin NO_y product. Relative differences between theory *a* and ACE-FTS in all the latitude/season bins are shown in Fig. 7. Since HNO_3 is totally dominating at altitudes below 20 km (Fig. 1) and since SMR HNO_3 measurements are corrected to match ACE-FTS HNO_3 (through Eq. 1), the systematic difference between ACE-FTS NO_y and Odin NO_y is consequently expected to be small for these altitudes. (The systematic difference is not zero because the coincidences are split into different latitude/season bins while the correction function is based on all latitude/seasons and because the correction is purely based on concentration with no altitude separation.) For higher altitudes, the Odin NO_y is consequently less dependent on this HNO_3 tuning.

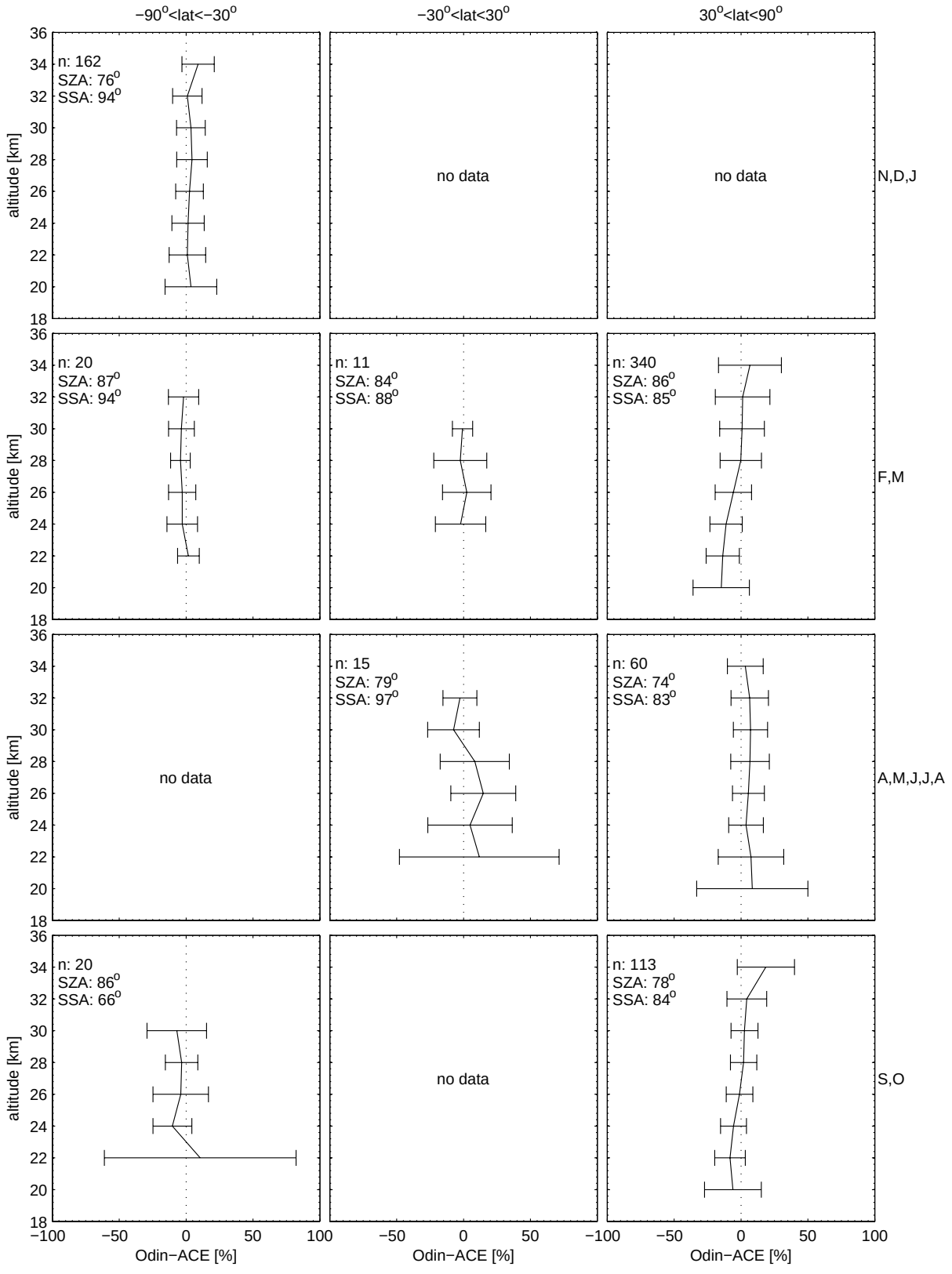

Fig. 7. NO_y results from Odin and ACE coincidences in 2004–2006, divided into 12 latitude/season bins and expressed as the mean (solid line) and 1σ standard deviation (error bars) of the relative differences (Odin-ACE/ACE). The average solar zenith angle (SZA) and solar scattering angle (SSA) are given together with the number of coincidences (n) in each bin.

3.3 Creating the climatology

The climatology comprises monthly zonal mean and the 1σ standard deviation (STD) of the Odin NO_y proxy data (theory a) from January 2002 to December 2006. It is expressed in number densities or volume mixing ratio as a function of latitude or equivalent latitude (EqL) on three independent vertical grids as specified below:

- **Concentration**:
  - Volume mixing ratio [ppb]
  - Number density [molecules cm^{-3}]
- **Horizontal grid (36 elements)**:
  - Latitude [deg]: 90° S–90° N in steps of 5
  - EqL [deg]: 90° S–90° N in steps of 5
- **Vertical grid (17 elements)**:
  - Altitude [km] : 14–46 in steps of 2
  - Pressure [hPa]: $10^3 \cdot 10^{-[\text{Altitude grid}]/16}$
  - Potential temperature [K]: 450–1650 in steps of 75

This makes in total 12 different datasets containing 3 dimensional matrices of mean and STD, each with $36 \times 17 \times 12$ grid cells. Note that the vertical grid spacing is chosen to correspond to equidistant altitudes which gives an exponential pressure grid (with a typical atmospheric scale height of 16 km). Conversion from number density to mixing ratio and from altitudes to pressure or potential temperature temperature are done using ECMWF data (altitude, pressure and temperature) which are also used as a background atmosphere for the OSIRIS and SMR retrievals. Furthermore, EqLs are calculated for each vertical grid cell by using ECMWF PV data. Note that each profile is interpolated to the fixed vertical and horizontal grids using independent pressure, temperature and PV information. Hence, the conversion between the different datasets must be done on a single profile basis and not on climatological means and STDs.

In order to restrict the climatology to regions where most of the information comes from the measurement and not from the a priori, only Odin data with measurement response larger than 0.5 are used. Using a higher response threshold will reduce the vertical range. In addition, to obtain useful means and STDs, the minimum number of profiles in each grid cell is set to 15. Altogether around 200 000 profiles are used in the climatology. The use of Gaussian statistics is supported by the concentration distributions within the climatology bins (not shown).

3.4 Uncertainty estimates

It is crucial that the box model correctly describes the NO_y partitioning. This issue is examined in Appendix A through comparisons with the JPL-MkIV interferometer.

Much less important is the use of a correct NO_y profile in the box model as to a first-order the partitioning is independent of the assumed NO_y, as long as it is correct within 50% or so. This is illustrated in Fig. 4 which shows that the effect on NO_y partitioning when the box model NO_y is perturbed by scaling the entire profile by -0.6 (-60%) to +0.6 (+60%). This perturbation represents the largest 1σ STD in the Odin NO_y climatology (see Sect 4.1). Considering first an example at 45° N and 28 km (upper panel) on 15 March, the largest change in partitioning is for $ClONO_2$ which shifts by 0.05; NO and NO_2 are virtually unchanged, and changes of about 0.03 are found for HNO_3 and $2 \times N_2O_5$. Note that this covers a factor of 4 in NO_y. More relevant than how $ClONO_2$ and $2 \times N_2O_5$ vary is their sum as these species are scaled together: their sum varies by only 0.02 over this range. The upper panel shows the variation at one altitude, latitude, and day and in this example the maximum shift between -0.6 and 0 and 0 and +0.6 would be 0.03 (considering NO, NO_2, HNO_3, and $ClONO_2$+$2 \times N_2O_5$). In the lower panel all altitudes, latitudes, and months are considered. The maximum shift in partitioning between -0.6 and 0 and 0 and +0.6 over NO, NO_2, HNO_3, and $ClONO_2$+$2 \times N_2O_5$ is plotted as a function of latitude and altitude. These represent the maximum over all months (calculated for day 15). Maximum shifts are generally found to be about 0.05 or smaller in the region of interest, with some larger values near the south pole at 18 km. The variability found in NO_y, shown later in Fig. 10, is generally less than 40% and so the lower panel in Fig. 4 represents a worst-case scenario, with the possible exception of the SH lower stratosphere. Hence, although the NO_y input is not believed to be entirely accurate, this is not a major source of uncertainty in the Odin NO_y data. Other sources of error in the photochemical box model such as an incomplete chemistry, errors in the photochemical rate data, or other model inputs will add uncertainties to the Odin NO_y data. However, based on the comparisons presented in Appendix A, any systematic errors over the altitude range of interest (15–40 km) appear to be minor and so it is concluded that the modeled partitioning is not a large source of systematic error.

Measurement uncertainties (random and systematic) in the OSIRIS and SMR instruments will propagate through the merging process (Eqs. 2 to 5) in a non-trivial way. Also model uncertainties will add to this in a way that is not fully understood. No attempt has been made to theoretically estimate the total uncertainties of the Odin proxy NO_y profiles. Instead, results from the ACE-FTS validation study, described in Sect. 3.2, are used to estimate the uncertainty.

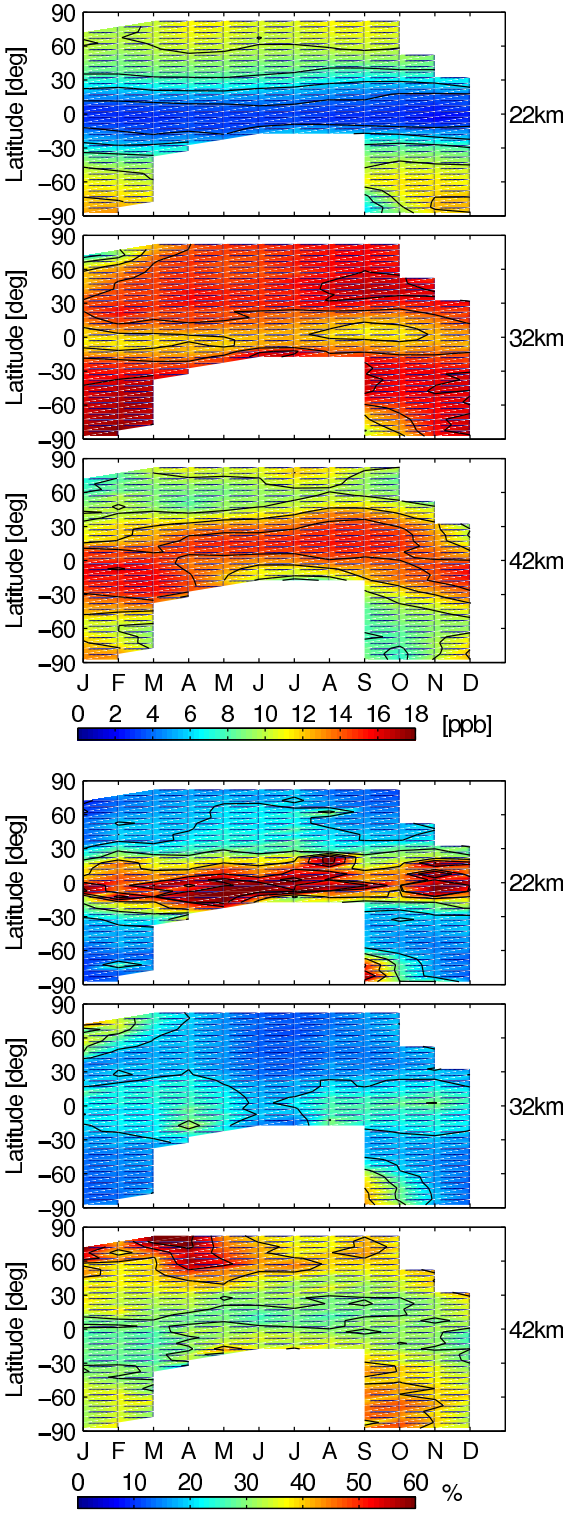

Fig. 8. Annual variation of NO_y mean volume mixing ratio [ppb] (upper panel) and 1σ standard deviation [%] (lower panel) of the Odin proxy climatology at three different altitude levels as a function of latitude [deg]. White regions represent periods and regions without data coverage.

The mean of the relative difference between Odin proxy NO_y and ACE observations is within 20% in all the latitude/season bins (see Fig. 7) which corresponds to around 1 ppb except for F-M northern latitudes below 25 km where it corresponds to around 2 ppb (not shown). The standard deviation of the mean difference is within 15% (1σ) if ignoring bins with very few coincidences and altitude below 22 km in A-M-J-J-A, see Fig. 7. These results indicate that the precision (random) and accuracy (systematic) of the Odin NO_y proxy data is 15% and 20% respectively, if ACE is assumed to be unbiased with zero noise and no real atmospheric differences exist between the co-located Odin and ACE measurements. Since noise in the ACE measurement and atmospheric variability will add to the standard deviation of the differences, the actual Odin NO_y precision is probably higher than the value given above although this is difficult to quantify.

Regarding the NO_y climatological monthly means, the random uncertainty is almost entirely averaged out, leaving only the systematic uncertainty of 20%. The climatological STD is driven by natural NO_y variability in conjunction with random uncertainties in the Odin measurements and in the photochemical box model. Thus, the climatological monthly STDs must be considered upper limit estimates of the true (atmospheric) STDs.

4 Results and discussion

4.1 Odin climatology

The Odin NO_y climatology generally covers the summer hemisphere but gives near-global coverage around the equinoxes (see Fig. 8). Furthermore, no information is available in the extreme 85° N to 90° N latitude bin due to Odin's orbit. This is not the case for the Southern Hemisphere where scheduled off-plane pointing provides enough data for the climatology. In altitude, the coverage is usually limited (due to low measurement response) to between 22 and 42 km at low latitudes and 20 to 40 km at high latitudes.

The monthly mean NO_y fields, shown in Figs. 8 and 9, show a peak (in mixing ratio) at around 38 km in the tropics and at around 30 km at mid-latitudes. Exceptions are the winter/spring polar regions where low concentrations are found throughout the stratosphere associated with descent of air in the vortex and heterogeneous denitrification processes on PSC particles at the lowest altitudes in the Antarctic vortex. The extremely low concentrations in September and October south of 60° S below 22 km corresponds to the region where PSCs are most frequently found (since June, July and August are not covered by OSIRIS). Note, however, that larger errors are expected during polar winter/spring due to increasing partitioning errors in the presence of PSCs since they are not represented by the photochemical box model (see Sect 2.3). Hence artifacts in the Odin proxy NO_y cannot be totally ruled

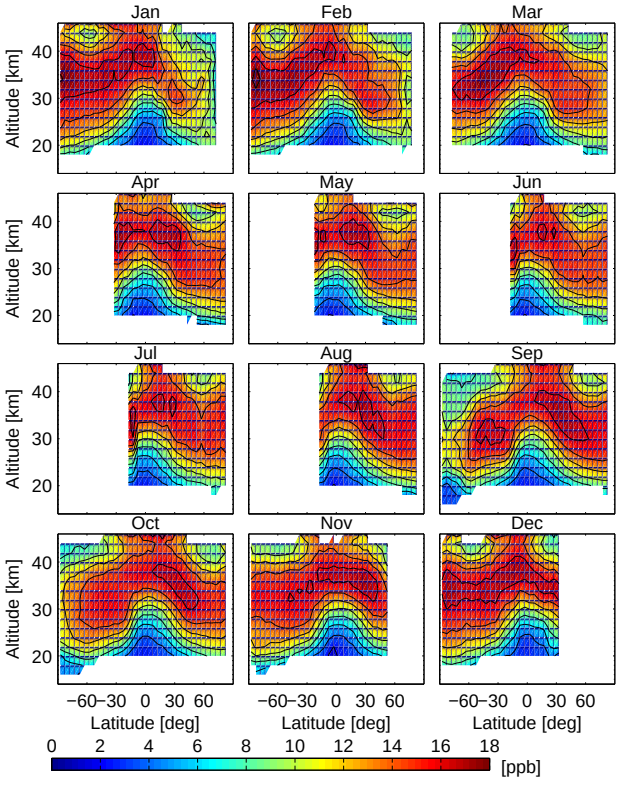

Fig. 9. Odin proxy NO_y monthly mean mixing ratios [ppb] as a function of latitude [deg] and altitude [km]. White regions represent no data.

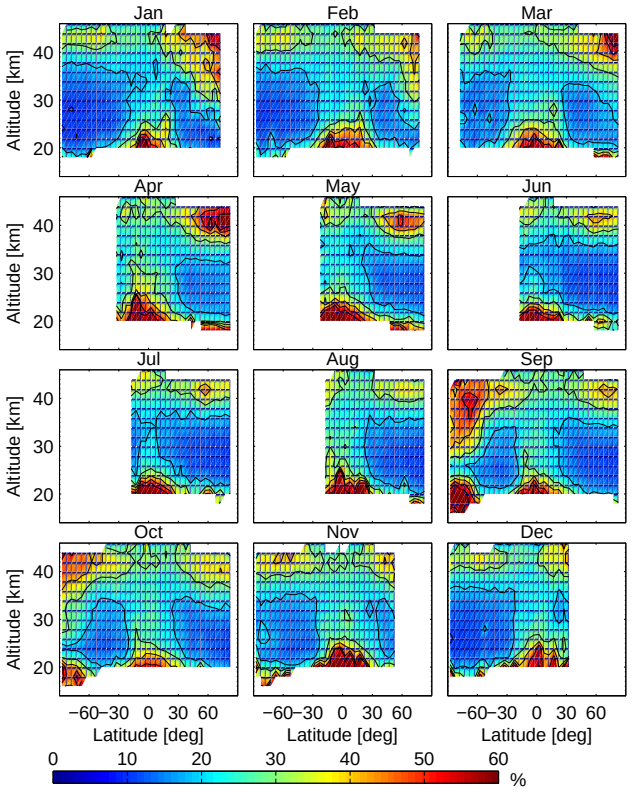

Fig. 10. Odin proxy NO_y monthly 1σ standard deviations in percent as a function of latitude [deg] and altitude [km]. White regions represent no data.

out in these regions. Possible signs of re-nitrification are also found when comparing the lowest altitudes of October and November during the southern polar spring. To conclude, the Odin proxy climatology seems consistent with the general understanding of the NO_y chemistry as introduced in Sect. 1.

The monthly 1σ STD seen in Fig. 10 is generally between 10 and 30%, except for winter and spring high latitudes above 30 km where values are well above 40%. This is probably due to occasional downward transport of mesospheric NO_x-rich air (see Sect. 4.3). Large STDs are also found in the tropical lower stratosphere, which are probably related to enhanced measurement uncertainties from water vapor, clouds and aerosol combined with very low NO_y abundances. Furthermore, the high STD (in percent) inside the southern polar vortex can be understood from the inter-annual variability of denitrification and due to the extremely low concentrations (close to zero) occasionally found here. The STD when viewed in ppb (not shown) are significantly less pronounced in this region.

The annual cycle (Fig. 8) is generally weak due to the long lifetime of NO_y. The only exception is found in the polar regions at low altitudes where denitrification occurs. The observed SMR HNO_3 enhancement in middle/upper stratosphere of the polar winter hemisphere (Urban et al., 2007) can not be seen in the Odin NO_y data because OSIRIS does not make night-time measurements.

4.2 Comparisons with other NO_y data sets

The Odin NO_y climatology is compared with output from the CMAM model and data sets from other instruments. As correlative ACE-FTS measurements have been utilized previously in the evaluation of the merging methodologies and for correction of SMR HNO_3 data they are not presented here since they are not an independent data source.

In general, the CMAM and Odin climatologies agree to within 20% or 2 ppb throughout the stratosphere, with CMAM generally larger than Odin in the upper stratosphere and smaller in the lower stratosphere. This is shown in Fig. 11. The major exceptions to the general good agreement occur in the polar regions. As discussed in Sect. 2.4 a numerical problem in the model simulation leads to unphysical NO_y values in a limited region southward of 50° S below 10 hPa from September to January. Hence the CMAM data is not shown in this region (gray boxes in Fig. 11).

Above 10 hPa during the Antarctic spring (September), CMAM displays lower NO_y values than Odin, suggestive of too strong downward transport of air in the model. This

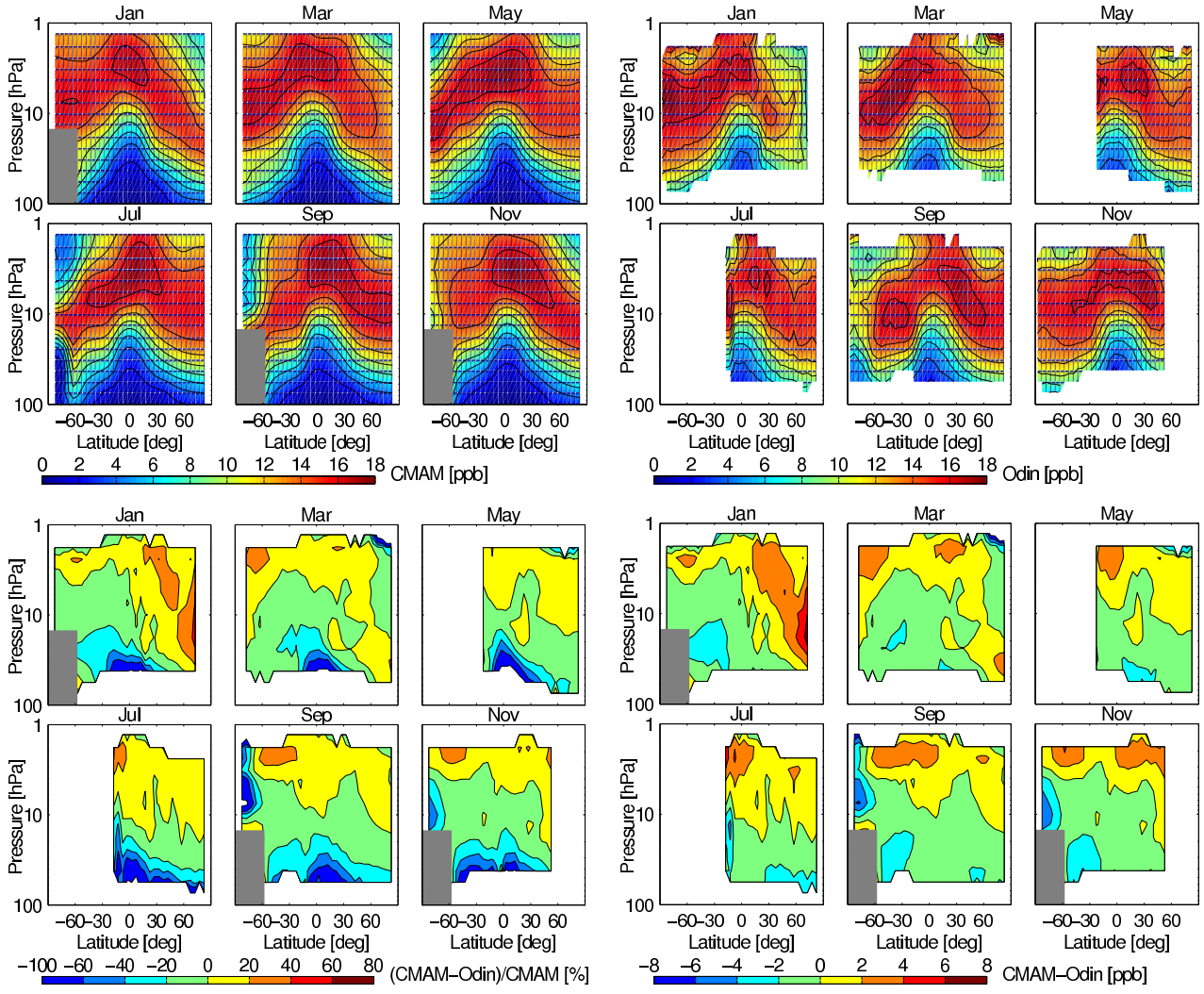

Fig. 11. CMAM simulated NO_y mixing ratios (ensemble average) [upper left panel] and Odin proxy NO_y climatology [upper right panel] as a function of latitude [deg] and pressure [hPa] for six selected months. Difference between the Odin and CMAM climatologies in percent [lower left panel] and absolute numbers [lower right panel]. CMAM data in the region southward of 50° S below 10 hPa during September to January are greyed out due to a numerical problem in the model (see Sect. 2.4)

is consistent with slightly warmer temperatures in CMAM in this region during spring as compared to other models and data assimilation products (Eyring et al., 2006). Note however that polar descent in CMAM during the winter season (June–August), which the Odin climatology does not cover, appear quite realistic (Eyring et al., 2006; Hegglin and Shepherd, 2007). It is also well known that current CCMs, including CMAM, display a too late spring vortex breakup in the Southern Hemisphere, which could explain part of the smaller NO_y concentrations at high southern latitudes during November (Fig. 11). The CMAM data show very low NO_y levels in the lower southern polar vortex during winter (July), where NO_y is almost entirely removed from the gas phase by sequestering HNO_3 in PSC particles. Unfortunately the Odin climatology does not cover this period, but low NO_y values in this region are still seen later in the season (September).

The differences in excess of 20% and 2 ppb in January at high northern latitudes are caused by the high degree of variation in this region. Considering the extensive interannual and decadal scale dynamical variability at the Northern Hemisphere high latitudes (see e.g. Butchart et al., 2000) and the relative shortness of the Odin data set, some disagreement can be expected here. Accordingly, the difference in this region and period is expected to be less when viewed in EqLs. A comparison between the Odin NO_y climatology based on EqLs (not shown) and the Odin NO_y climatology based on pure latitudes show significant differences only at the edge of the Arctic vortex but small differences elsewhere, including the northern most latitudes where the Odin-CMAM disagreement is largest. This indicates that the CMAM differences will not completely disappear when switching to EqLs in Fig. 11. Unfortunately this cannot be

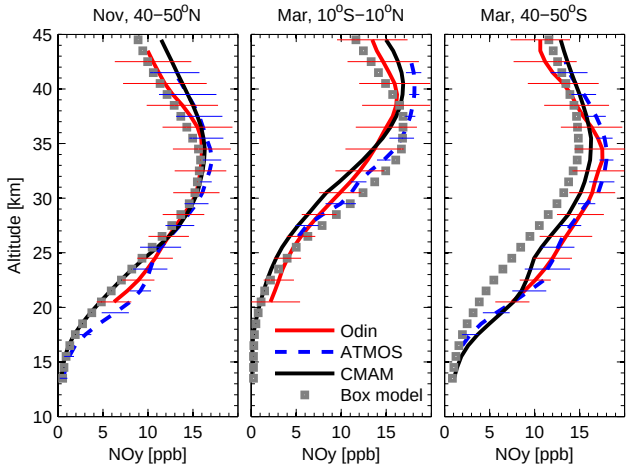

Fig. 12. Mean NO_y profiles for three month/latitudes of Odin proxy (black thick line), ATMOS observation (grey thick line), CMAM simulations (dashed line) and the NO_y used to initialize the photochemical box model (boxes). The error bars indicate the 1σ standard deviation for the ATMOS and Odin data sets.

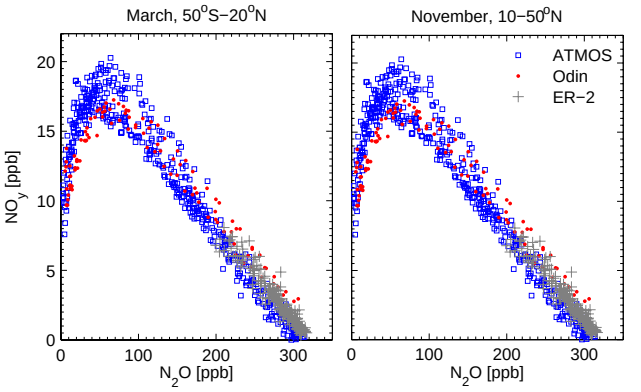

Fig. 13. N_2O:NO_y correlation of the Odin proxy NO_y and SMR N_2O data (red dots), ATMOS observations (blue squares) and ER-2 flight measurements (grey crosses) for two different months and latitude bands. Note that ER-2 only gives low altitude data.

investigated further since the CMAM data provided for this study do not contain the PV information needed to calculate the EqLs. Note also that all data from this region and period correspond to off-axis measurements in 2003 with expected increased OSIRIS measurement uncertainty, see Sect. 4.3.

The large relative differences in the tropical lower stratosphere (left lower panel of Fig. 11) are of little relevance since the NO_y concentrations are very small in this region and absolute differences (right lower panel) are reasonable. Note that CMAM data, in addition to the five species considered for the Odin climatology, also includes $BrONO_2$, NO_3 and HO_2NO_2. These gases, however, do not contribute significantly (0–2% in total) to the NO_y concentrations at the Odin daytime measurements (see Fig. 1).

Odin NO_y was also compared to measurements from the ATMOS experiment (Gunson et al., 1996), a predecessor of the ACE-FTS. Like ACE, ATMOS is a Fourier-transform interferometer that measures solar absorption at a spectral resolution of 0.01 cm^{-1} between 600 and 4800 cm^{-1}. ATMOS flew on the space shuttle on four occasions (1985, 1992, 1993, and 1994) and collected about 350 occultations. While there is no temporal overlap between these two data sets, a comparison is still appropriate especially as ATMOS NO_y has become a de facto benchmark. ATMOS version 3 data is employed here (Irion et al., 2002). The ∼15 year difference between ATMOS and Odin should only amount to around 5% difference based on recent trends in N_2O and model studies (McLinden et al., 2001). Due to the intermittent nature of the ATMOS observations there are only three months/latitudes in which sufficient data exist to provide meaningful averages. These are November, 40–50° N, March, 10° S–10° N, and March 40–50° S. ATMOS NO_y was computed by simply adding together the big five NO_y species, analogous to the procedure applied to ACE-FTS.

Figure 12 shows a comparison between the ATMOS mean NO_y and the Odin NO_y for each month/latitude mentioned above. Also included in the comparison are the CMAM mean NO_y and the NO_y used to initialize the box model (Olsen et al., 2001). In each case the four NO_y sources show similar behavior but with ATMOS and Odin being the most consistent with the exception of some differences at 40 km for March, 10° S–10° N. Also, both CMAM and the box model NO_y tend to be smaller in the lower stratosphere, particularly for March, 40–50° S, where CMAM is lower by ∼3 ppb and the box model by up to 6 ppb than ATMOS and Odin.

Another method of evaluating the Odin NO_y is to examine its correlation with N_2O. It is well known that a compact relationship exists between N_2O and NO_y (Keim et al., 1997). A monthly-mean SMR N_2O climatology was generated in a fashion analogous to the Odin NO_y, using SMR version 2.1 data (considering only profiles with QUALITY FLAG=0 and individual points with a measurement response of 0.75 or larger) (Urban et al., 2005a,b, 2006). SMR N_2O is thoroughly validated and is found to be in very good agreement with various correlative data sets (Urban et al., 2005a, 2006; Lambert et al., 2007; Strong et al., 2008). Figure 13 shows the N_2O:NO_y correlation derived from Odin and ATMOS data for two month/latitude bands. These expanded latitude bands, as compared to the profile comparison in Fig. 12, were chosen to incorporate additional ATMOS data into in the comparisons. Also plotted are N_2O and NO_y climatologies derived from numerous NASA ER-2 high altitude research aircraft flights (Strahan, 1999) although these data correspond only to the lower stratosphere (≤20 km). The overall

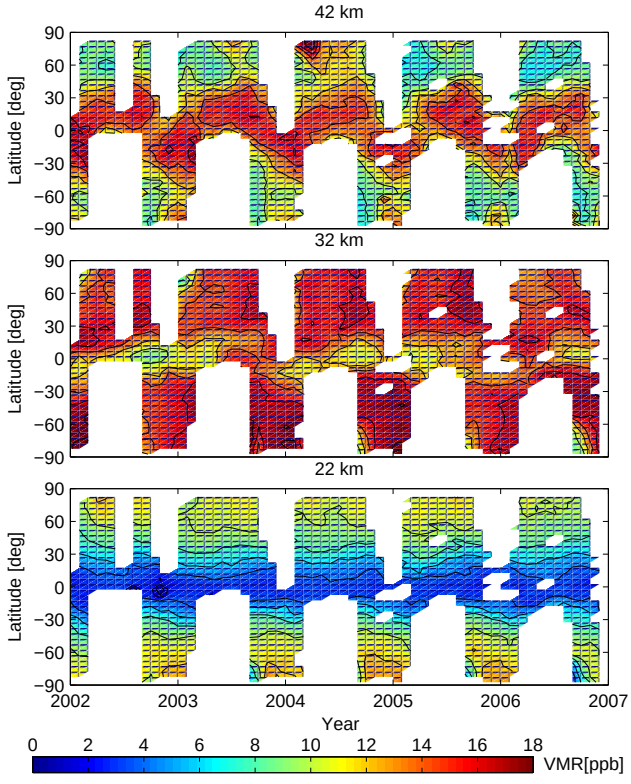

Fig. 14. Odin proxy NO_y monthly mean mixing ratios [ppb] from January 2002 to December 2006 at 22, 32 and 42 km. White regions represent periods and regions without data coverage.

relationships appear quite similar between the three data sets except at the lowest N_2O values in March where some Odin NO_y is seen to fall off faster than ATMOS. Some of this may be due to a sampling bias in the ATMOS data as a larger fraction of this data is in the mid-latitudes. The lower stratosphere (320 ppb$<[N_2O]<$150 ppb) correlation slopes of these N_2O:NO_y datasets, restricted to mid-latitudes to remove any sampling biases, have been calculated. For March, 50° S–30° S the Odin, ATMOS, and ER-2 values are −0.071, −0.074, and −0.065, respectively. For November, 30° N–50° N, they are −0.072, −0.073, and −0.067, respectively. These values, consistent with each other, are also in good agreement with other measurements (Olsen et al., 2001).

4.3 Odin NO_y time series

While not a major focus of this paper, it is worthwhile examining the Odin NO_y time series and its inter-annual variability. Figure 14 shows the five-year monthly-mean time series at altitudes of 22, 32, and 42 km. Note that the latitudinal coverage and the number of measurement days per month vary from year to year. Of particular interest is that all northern latitude measurements in January are from 2003 when Odin was pointed off the orbital plane into sunlight in order to provide OSIRIS data. Hence, this region should be treated with caution since it does not contain multi-year averages and due to extreme observation angles which may increase OSIRIS measurement errors.

There are also several NO_y inter-annual differences. The most striking feature is the high altitude maximum at the northern polar latitudes in March and April 2004 (see the 42 km level in Fig. 14). This is evidence of enhanced NO_x (e.g. Seppälä et al., 2004; Randall et al., 2005; Funke et al., 2005a; Orsolini et al., 2005) and HNO_3 (Stiller et al., 2005) following the strong subsidence of NO_x-rich upper atmospheric air within the particularly intense polar vortex in the beginning of 2004 (Manney et al., 2005). The magnitude of this enhancement in the Odin data should be treated with caution since the NO_x is mainly in NO and not in the measured NO_2 or HNO_3 at these altitudes (see Fig. 1). Also of note are frequent minima at the southern polar latitudes around September–October due to the heterogenous removal of gas-phase NO_y. Lowest minimum is found in 2006 and highest in 2002, consistent with the major Antarctic stratospheric warming that year (Ricaud et al., 2005). Furthermore, there is possibly a signal related to the QBO (quasi biennial oscillation) in the tropics at 32 km which seems correlated (in-phase) with SMR N_2O observations (not shown) which indicate a clear QBO response. A signal in N_2O is likely to transform into a signal in NO_y but an in-depth study of this is beyond the scope of this work.

4.4 Outlook

As mentioned before, the Odin proxy NO_y product may be useful in studies of the stratospheric nitrogen chemistry, as initialization to atmospheric models or to validate model outputs. The CMAM comparison in this study indicates a low bias in NO_y levels in the southern polar upper stratosphere during spring. In addition, the comparison has helped to identify a significant numerical problem in the treatment of NO_y in the presence of PSCs during the spring which could compromise the skill in predicting future atmospheric states, particularly the Antarctic ozone recovery (WMO, 2007; Shepherd and Randel, 2007).

Future work will include comparisons with several CCMs and CTMs (Chemical Transport Models) to study whether the CMAM biases are occuring also in other atmospheric models. Improvements in the Odin/SMR HNO_3 retrieval code related to identified spectroscopic and calibration issues should eliminate the need for a systematic correction of SMR HNO_3 and make the Odin NO_y a more independent data source. Furthermore, SMR is making NO observations one day a month (since October 2003) and analysis and validation of this data product is ongoing. NO will be a welcomed addition to the proxy Odin NO_y climatology at high altitudes where the NO_2 concentration is low, see Fig. 1.

5 Data access

The NO_y climatology can be freely downloaded through the OSIRIS web-site at University of Saskatchewan: http://osirus.usask.ca or directly provided by the main author samuel.brohede@chalmers.se.

6 Conclusions

Five years of OSIRIS NO_2 and SMR HNO_3 data from the Odin satellite have been merged to construct a stratospheric proxy NO_y product using a photochemical box model to compensate for the missing NO_y species. ACE-FTS observations of the big five NO_y species (NO, NO_2, HNO_3, $2\times N_2O_5$ and $ClONO_2$) are used to evaluate the merging method. The advantage of the Odin NO_y data set is higher temporal and spatial coverage compared to ACE occultation measurements.

Several approaches to merge NO_2 and HNO_3 were studied. Best agreement between the Odin NO_y proxy and ACE-FTS measurements was achieved when OSIRIS NO_2 is used to estimate NO and a weighted average of SMR HNO_3 and OSIRIS NO_2 is used to estimate N_2O_5 and $ClONO_2$. It is clearly shown that any way to merge the two Odin data sets gives a more accurate NO_y product than using data from only one of the Odin instruments. SMR data were corrected for a known systematic high bias. The random and systematic uncertainties for an individual Odin NO_y profile are estimated to be around 15 and 20%, respectively.

The Odin NO_y climatology is based on daytime measurements and contains monthly mean and standard deviation expressed as mixing ratio or number density as a function of latitude or equivalent latitude (5°bins) on 17 vertical layers (altitude, pressure or potential temperature) between 20 and 40 km. The coverage is generally limited to the summer hemisphere but gives near-global coverage around the equinoxes.

Monthly means show a maximum at around 38 km in the tropics and at around 30 km at latitudes higher than 30°. Exceptions are the winter/spring polar regions where low concentrations are found throughout the stratosphere associated with descent of air in the vortex and heterogeneous processes involving PSCs. The monthly 1σ STD is generally between 10 and 30%, except for winter and spring high latitudes above 30 km where values are well above 40%. The year to year variation reveals enhanced NO_x in early 2004 at 42 km, following the strong subsidence of NO_x-rich upper atmospheric air within the particularly intense polar vortex in the beginning of 2004. The slope of the Odin N_2O:NO_y correlation in the lower stratosphere ($320\,ppb<[N_2O]<150\,ppb$) was found to be -0.07, in good agreement with ATMOS and ER-2 measurements.

The agreement with CMAM simulated fields are within 20% or 2 ppb throughout most of the stratosphere except in the proximity of the polar vortex. Particularly, large disagreements within the Antarctic vortex indicate too strong descent of air in the upper stratosphere during the spring season in the model. A numerical problem in CMAM, leading to unphysically high NO_y values southward of 50° S below 10 hPa from September to January, was also identified during the course of this study.

The combination of temporal and spatial coverage, length of data record, and accuracy and precision make Odin NO_y a valuable product for process studies, model assessments, and perhaps even trend analyses.

Appendix A

Uncertainty in the NO_y partitioning of the photochemical box model

To evaluate the ability of the photochemical box model (see Sect. 5.2; Brohede et al. (2007a) and Appendix A; Brohede et al., 2007c) to correctly simulate the NO_y partitioning, comparisons are made against profiles measured by the JPL MkIV interferometer on 10 balloon flights between 1997–2005. The MkIV interferometer is a high resolution ($0.01\,cm^{-1}$) Fourier Transform Infra-Red (FTIR) spectrometer and is based largely on that of ATMOS (Toon, 1991). It measures sunlight transmitted through the atmosphere between 650 to $5650\,cm^{-1}$ and thus captures the entire mid-infrared. From these spectra, stratospheric profiles of over 30 trace species are retrieved at a vertical resolution of 2–3 km, including all important members of the NO_y family (Sen et al., 1998; Osterman et al., 1999). The MkIV is chosen for this purpose as it represents an independent, high-quality data set that has been analyzed extensively and used in numerous validation studies (Toon et al., 2002).

To simulate a MkIV profile, the box model is initialized with the MkIV-measured neutral density, temperature, ozone, and NO_y (calculated by summing the individual NO_y species) profiles. The model latitude is taken from the latitude at the location of the MkIV 25 km tangent altitude. All other model inputs are as described in Sect. 2.3. The MkIV and model abundances of the NO_y family members are compared in Fig. A1. They are plotted on a linear scale to highlight the level of agreement at larger mixing ratios. For most flights, the agreement is very good with the model capturing the transition from HNO_3 being dominant in the lower stratosphere to NO_x in the upper stratosphere. The two exceptions to this are in the polar winter on Julian days 337 (1999) and 350 (2002) above 25 km, and to a lesser extent day 75 (2000) in polar spring. In these cases the model predicts too much HNO_3. This is likely due to the steady-state nature of the model which is unable to capture any air mass history. During this period, on the edge of the polar night, any air mass which is exposed to an appreciable amount of sunlight, especially in the upper stratosphere, will rapidly lose HNO_3 to the more reactive species. For each of these cases 10-day back trajectories were computed using the HYSPLIT4 dispersion model (Draxler and Rolph, 2003; Rolph, 2003) to determine the history of the airmasses. On day 337 (1999) air above 25 km was over the pole two days prior and was north of 75° for a week prior to that, and so was exposed to continual sunlight during this period, sufficient to destroy HNO_3 at these altitudes. The situation for day 350 (2002) is not as conclusive. During the 10-days prior to the balloon flight, airmasses above 20 km were found to move from latitudes between 60 and 90° N. Day 75 (2000) reveals an airmass history which is spent northward of the observation latitude. In this springtime case the lack of PSCs in the photochemical box model may also have an impact on an model-measurement differences. The impact of these discrepancies should be mitigated as the Odin climatology it is based on an average over many profiles. Moreover, OSIRIS does not sample the winter hemisphere which should avoid the worst of these periods.

Also plotted in Fig. A1 are the NO_x/NO_y ratios. This is an important quantity since of all the missing NO_y species, NO is by far the most important and it is determined solely by NO_2. Here too there is generally good agreement with the MkIV profiles with the obvious exception of Julian days 337 and 350 above 25 km.

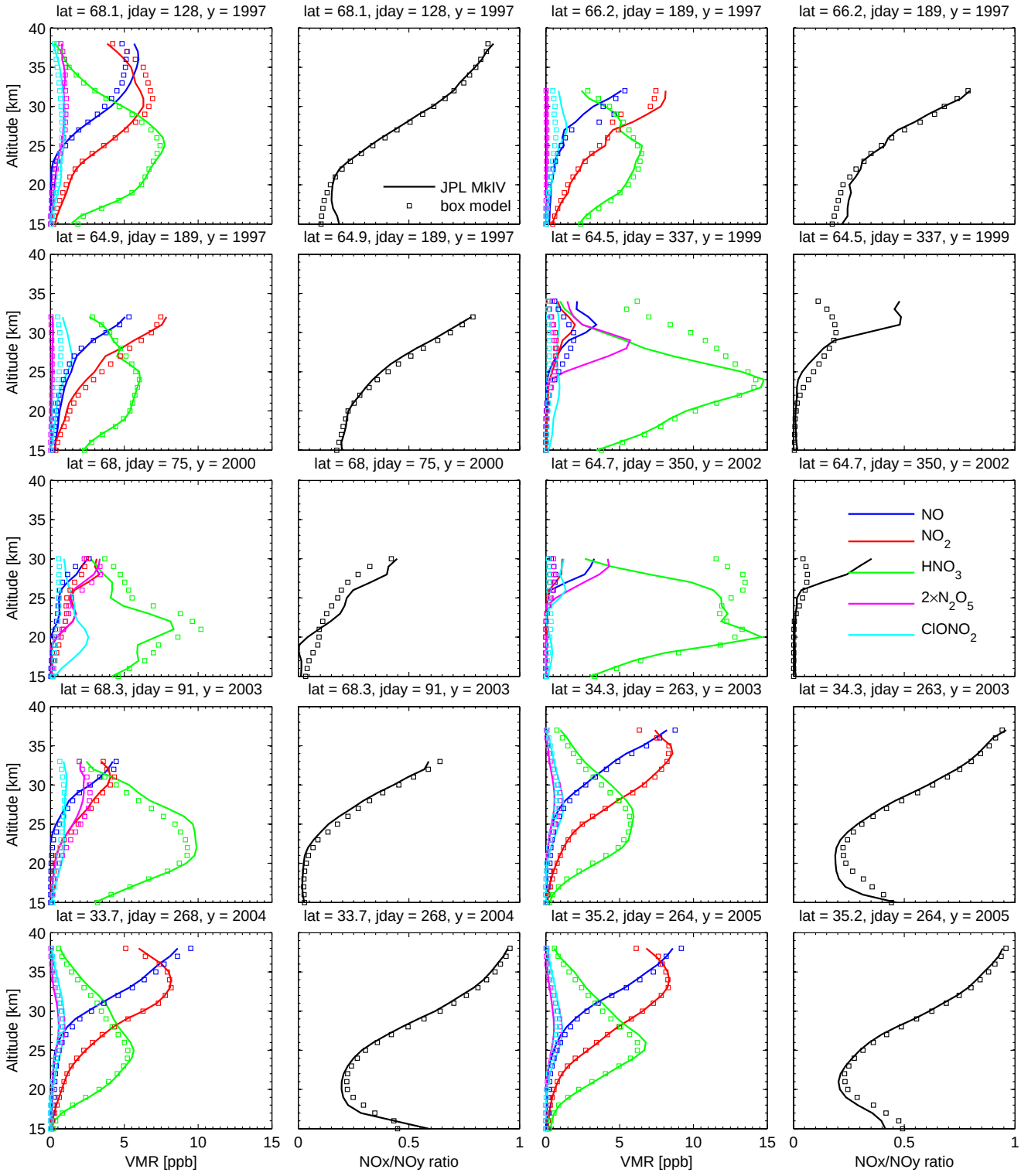

Fig. A1. Comparison of photochemical box model output (boxes) with MkIV balloon measurements (solid lines) of the big five NO_y species (NO, NO_2, HNO_3, $2N_2O_5$, $ClONO_2$) and NO_x/NO_y ratios for 10 flights between 1997–2005. The box model is initialized with the MkIV-measured neutral density, temperature, ozone, and NO_y profiles. All other model inputs are as described in Sect. 2.3.

Acknowledgements. This work is supported by the Swedish National Space Board and Chalmers University of Technology. Odin is a Swedish-led satellite project funded jointly by Sweden (SNSB), Canada (CSA), Finland (TEKES), France (CNES), and supported since 2007 by the third party mission programme of the European Space Agency (ESA). The CMAM data in this paper were provided by the Canadian Stratospheric Processes and their Role in Climate Network (C-SPARC), funded by the Canadian Foundation for Climate and Atmospheric Sciences and the Canadian Space Agency. Funding for the ACE mission was provided primarily by the Canadian Space Agency (CSA) and the Natural Sciences and Engineering Research Council (NSERC) of Canada.The authors gratefully acknowledge the NOAA Air Resources Laboratory (ARL) for the provision of the HYSPLIT transport and dispersion model and the READY website (http://www.arl.noaa.gov/ready.html) used in this publication. NCEP reanalysis data are provided by the NOAA/OAR/ESRL PSD, Boulder, Colorado, USA, from their website at http://www.cdc.noaa.gov/. Finally, we thank the reviewers for their constructive comments.

Edited by: V. Fomichev

References

Beagley, S. R., de Grandpré, J., Koshyk, J. N., McFarlane, N. A., and Shepherd, T. G.: Radiative-dynamical climatology of the first-generation Canadian Middle Atmosphere Model, Atmos. Ocean, 35, 293–331, 1997.

Bernath, P. F., McElroy, C. T., Abrams, M. C., Boone, C. D., Butler, M., Camy-Peyret, C., Carleer, M., Clerbaux, C., Coheur, P.-F., Colin, R., DeCola, P., DeMazieŕe, M., Drummond, J. R., Dufour, D., Evans, W. F. J., Fast, H., Fussen, D., Gilbert, K., Jennings, D. E., Llewellyn, E. J., Lowe, R. P., Mahieu, E., McConnell, J. C., McHugh, M., McLeod, S. D., Michaud, R., Midwinter, C., Nassar, R., Nichitiu, F., Nowlan, C., Rinsland, C. P., Rochon, Y. J., Rowlands, N., Semeniuk, K., Simon, P., Skelton, R., Sloan, J. J., Soucy, M.-A., Strong, K., Tremblay, P., Turnbull, D., Walker, K. A., Walkty, I., Wardle, D. A., Wehrle, V., Zander, R., and Zou, J.: Atmospheric Chemistry Experiment (ACE): Mission overview, Geophys. Res. Lett., 32, L15S01, doi:10.1029/2005GL022386, 2005.

Bourassa, A. E., Degenstein, D., Gattinger, R. L., and Llewellyn, E.: Stratospheric aerosol retrieval with optical spectropraph and infrared imaging system limb scatter measurements, J. Geophys. Res., 112, D10217, doi:10.1029/2006JD008079, 2007.

Brasseur, G. and Remsberg, E.: Summary of the MMII Intercomparisons for Chemistry, in: Models and Measurements Intercomparison II, edited by: Park, J. H., Ko, M. K. W., Jackman, C. H., Plumb, R. A., Kaye, J. A., and Sage, K. H., NASA Langley Research Center, 190–306, 1999.

Brohede, S., Haley, C. S., McLinden, C. A., Sioris, C. E., Murtagh, D. P., Petelina, S. V., Llewellyn, E. J., Bazureau, A., Goutail, F., Randall, C. E., Lumpe, J. D., Taha, G., Thomasson, L. W., and Gordley, L. L.: Validation of Odin/OSIRIS Stratospheric NO_2 Profiles, J. Geophys. Res., 112, D07310, doi:10.1029/2006JD007586, 2007a.

Brohede, S., Jones, A., and Jégou, F.: Internal consistency in the Odin stratospheric ozone products, Can. J. Phys., 85(11), 1275–1285, doi:10.1139/P07-142, 2007b.

Brohede, S., McLinden, C. A., Berthet, G., Haley, C. S., Murtagh, D., and Sioris, C. E.: A Stratospheric NO_2 Climatology from Odin/OSIRIS Limb-Scatter Measurement, Can. J. Phys., 85(11), 1253–1274, doi:10.1139/P07-141, 2007c.

Brühl, C., Steil, B., Stiller, G., Funke, B., and Jöckel, P.: Nitrogen compounds and ozone in the stratosphere: comparison of MIPAS satellite data with the chemistry climate model ECHAM5/MESSy1, Atmos. Chem. Phys., 7, 5585–5598, 2007, http://www.atmos-chem-phys.net/7/5585/2007/.

Butchart, N., Austin, J., Knight, J. R., Scaife, A. A., and Gallani, M. L.: The Response of the stratospheric climate to projected changes in the concentrations of well-mixed Greenhouse Gases from 1992 to 2051, J. Climate, 13, 2142–2159, 2000.

Danilin, M. Y. I., Koike, M., Yue, G. K., Jones, N. B., and Johnston, P. V.: Nitrogen species in the post-Pinatubo stratosphere: Model analysis utilizing UARS measurements, J. Geophys. Res., 104(D7), 8247–8262, doi:10.1029/1999JD900024, 1999.

de Grandpré, J., Sandilands, J. W., McConnell, J. C., Beagley, S. R., Croteau, P. C., and Danilin, M. Y.: Canadian middle atmosphere model: Preliminary results from the chemical transport module, Atmos. Ocean, 35(4), 385–431, 1997.

de Grandpré, J., Beagley, S. R., Fomichev, V. I., Griffioen, E., McConnell, J. C., Medvedev, A. S., and Shepherd, T. G.: Results from the Canadian Middle Atmosphere Model, J. Geophys. Res., 105, 26 475–26 491, 2000.

Degenstein, D. A., Llewellyn, E. J., and Lloyd, N. D.: Volume emission rate tomography from a satellite platform, Appl. Opt., 42(8), 1441–1450, 2002.

Dibb, J. E., Scheuer, E., Avery, M., Plant, J., and Sachse, G.: In situ evidence for renitrification in the Arctic lower stratosphere during the polar aura validation experiment (PAVE), Geophys. Res. Lett., 12, L12815, doi:10.1029/2006GL026243, 2006.

Draxler, R. R. and Rolph, G. D.: HYSPLIT (HYbrid Single-Particle Lagrangian Integrated Trajectory) Model access via NOAA ARL READY Website , NOAA Air Resources Laboratory, Silver Spring, MD, http://www.arl.noaa.gov/ready/hysplit4.html(last access: May 2008), 2003.

Eyring, V., Kinnison, D. E., and Shepherd, T. G.: Overview of planned coupled chemistry climate simulations to support upcoming ozone and climate assessments, SPARC Newsletter, 25, 11–17, 2005.

Eyring, V., Butchart, N., Waugh, D. W., Akiyoshi, H., Austin, J., Bekki, S., Bodeker, G. E., Boville, B. A., Bruühl, C., Chipperfield, M. P., Cordero, E., Dameris, M., Deushi, M., Fioletov, V. E., Frith, S. M., Garcia, R. R., Gettelman, A., Giorgetta, M. A., Grewe, V., Jourdain, L., Kinnison, D. E., Mancini, E., Manzini, E., Marchand, M., Marsh, D. R., Nagashima, T., Newman, P. A., Nielsen, J. E., Pawson, S., Pitari, G., Plummer, D. A., Rozanov, E., Schraner, M., Shepherd, T. G., Shibata, K., Stolarski, R. S., Struthers, H., Tian, W., and Yoshiki, M.: Assessment of temperature, trace species, and ozone in chemistry-climate model simulations of the recent past, J. Geophys. Res., 111, D22308, doi:10.1029/2006JD008281, 2006.

Eyring, V., Waugh, D. W., and Bodeker, G. E.: Multimodel projections of stratospheric ozone in the 21st century, J. Geophys. Res., 112, D16303, doi:10.1029/2006JD008332, 2007.

Fish, D. J., Roscoe, H. K., and Johnston, P. V.: Possible causes of stratospheric NO_2 trends observed at Lauder, Geophys. Res. Lett., 20, 3313–3316, doi:10.1029/2000GL011700, 2000.

Fischer, H., Birk, M., Blom, C., Carli, B., Carlotti, M., von Clarmann, T., Delbouille, L., Dudhia, A., Ehhalt, D., Endemann, M., Flaud, J. M., Gessner, R., Kleinert, A., Koopman, R., Langen, J., L´pez-Puertas, M., Mosner, P., Nett, H., Oelhaf, H., Perron, G., Remedios, J., Ridolfi, M., Stiller, G., and Zander, R.: MIPAS: an instrument for atmospheric and climate research, Atmos. Chem. Phys., 8, 2151–2188, 2008, http://www.atmos-chem-phys.net/8/2151/2008/.

Forster, P., Ramaswamy, V., Artaxo, P., Berntsen, T., Betts, R., Fahey, D., Haywood, J., Lean, J., Lowe, D., Myhre, G., Nganga, J., Prinn, R., Raga, G., Schulz, M., and Dorland, R. V.: Changes in Atmospheric Constituents and in Radiative Forcing, in: Climate change 2007: The physical scientific basis, Contribution of Working Group I to the Fourth Assessment Report of the Intergovernmental Panel on Climate Change, edited by: Solomon, S., Qin, D., Manning, M., Chen, Z., Marquis, M., Averyt, K. B., Tignor, M., and Miller, H., Cambridge University Press, Cambridge, United Kingdom and New York, NY, USA, 2007.

Frisk, U., Hagström, M., Ala-Laurinaho, J., Andersson, S., Berges, J.-C., Chabaud, J.-P., Dahlgren, M., Emrich, A., Florén, H.-G., Gredrixon, M., Gaier, T., Haas, R., Hirvonen, T., Hjalmarsson, A., Jakobsson, B., Jukkala, P., Kildal, P. S., Kollberg, E., Lassing, J., Lecacheux, A., Lehikoinen, P., Lehto, A., Mallat, J., Marty, C., Michet, D., Narbonne, J., Nexon, M., Olberg, M., Olofsson, A. O. H., Olofsson, G., Origné, A., Petersson, M., Piironen, P., Pons, R., Pouliquen, D., Ristorcelli, I., Rosolen, C., Rouaix, G., Räisänen, A. V., Serra, G., Sjöberg, F., Stenmark, L., Torchinsky, S., Tuovinen, J., Ullberg, C., Vinterhav, E., Wadefalk, N., Zirath, H., Zimmermann, P., and Zimmermann, R.: The Odin satellite I. Radiometer design and test, Astron. Astrophys., 402, L27–L34, doi:10.1051/0004-6361:20030335, 2003.

Funke, B., López-Puertas, M., Gil-López, S., von Clarmann, T., Stiller, G. P., Fischer, H., and Kellmann, S.: Downward transport of upper atmospheric NO_x into the polar stratosphere and lower mesosphere during the Antarctic 2003 and Arctic 2002/2003 winters, J. Geophys. Res., 110, D09 308, doi:10.1029/2005JD006463, 2005a.

Funke, B., Lopez-Puertas, M., von Clarmann, T., Stiller, G. P., Fischer, H., Glatthor, N., Grabowski, U., Höpfner, M., Kellmann, S., Kiefer, M., Linden, A., Tsidu, G. M., Milz, M., Steck, T., and Wang, D. Y.: Retrieval of stratospheric NO_x from 5.3 and 6.2 Mm nonlocal thermodynamic equilibrium emissions measured by Michelson Interferometer for Passive Atmospheric Sounding (MIPAS) on Envisat, J. Geophys. Res., 110, D09302, doi:10.1029/2004JD005225, 2005b.

Gille, J. C. and Russel, J. M. I.: The Limb Infrared Monitor of the Stratosphere: experiment description, performance, and results, J. Geophys. Res., 89(D4), 5125–5140, 1984.

Gunson, M. R., Abbas, M. M., Abrams, M. C., Allen, M., Brown, L. R., Brown, T. L., Chang, A. Y., Goldman, A., Irion, F. W., Lowes, L. L., Mahieu, E., Manney, G. L., Michelsen, H. A., Newchurch, M. J., Rinsland, C. P., Salawitch, R. J., Stiller, G. P., Toon, G. C., Yung, Y. L., and Zander, R.: The Atmospheric Trace Molecule Spectroscopy (ATMOS) experiment: Deployment on the ATLAS Space Shuttle missions, Geophys. Res. Lett., 23, 2333–2336, doi:10.1029/96GL01569, 1996.

Haley, C. S. and Brohede, S.: Status of the Odin/OSIRIS Stratospheric O_3 and NO_2 Data Products, Can. J. Phys., 85, 11, 1177–1194, doi:10.1139/P07-114, 2007.

Haley, C. S., Brohede, S. M., Sioris, C. E., Griffioen, E., Murtagh, D. P., McDade, I. C., Eriksson, P., Llewellyn, E. J., Bazureau, A., and Goutail, F.: Retrievals of stratospheric O_3 and NO_2 profiles from Odin Optical Spectrograph and InfraRed Imager System (OSIRIS) limb-scattered sunlight measurements, J. Geophys. Res., 109, D16303, doi:10.1029/2004JD004588, 2004.

Hegglin, M. I. and Shepherd, T. G.: O_3-N_2O correlations from the Atmospheric Chemistry Experiment: Revisiting a diagnostic of transport and chemistry in the stratosphere, J. Geophys. Res., 112, D19301, doi:10.1029/2006JD008281, 2007.

Irion, F. W., Gunson, M. R., Toon, G. C., Chang, A. Y., Eldering, A., Mahieu, E., Manney, G. L., and Michelsen, H. A.: Atmospheric Trace Molecule Spectroscopy (ATMOS) Experiment Version 3 data retrievals, Appl. Opt., 41(33), 6968–6979, 2002.

Keim, E. R., Loewenstein, M., Podolske, J. R., Fahey, D. W., Gao, R. S., Woodbridge, E. L., Wamsley, R. C., Donnelly, S. G., Negro, L. A. D., Nevison, C. D., Solomon, S., Rosenlof, K. H., Scott, C. J., Ko, M. K. W., Weisenstein, D., and Chan, K. R.: Measurements of the NO_y-N_2O correlation in the lower stratosphere: Latitudinal and seasonal changes and model comparisons, J. Geophys. Res., 102(D11), 13 193–13 212, doi:10.1029/96JD03921, 1997.

Kerzenmacher, T., Wolff, M. A., Strong, K., Dupuy, E., Walker, K. A., Amekudzi, L. K., Batchelor, R. L., Bernath, P. F., Berthet, G., Blumenstock, T., Boone, C. D., Bramstedt, K., Brogniez, C., Brohede, S., Burrows, J. P., Catoire, V., Dodion, J., Drummond, J. R., Dufour, D. G., Funke, B., Fussen, D., Goutail, F., Griffith, D. W. T., Haley, C. S., Hendrick, F., Höpfner, M., Huret, N., Jones, N., Kar, J., Kramer, I., Llewellyn, E. J., L´pez-Puertas, M., Manney, G., McElroy, C. T., McLinden, C. A., Melo, S., Mikuteit, S., Murtagh, D., Nichitiu, F., Notholt, J., Nowlan, C., Piccolo, C., Pommereau, J.-P., Randall, C., Raspollini, P., Ridolfi, M., Richter, A., Schneider, M., Schrems, O., Silicani, M., Stiller, G. P., Taylor, J., Tétard, C., Toohey, M., Vanhellemont, F., Warneke, T, Zawodny, J. M., and Zou, J.: Validation of NO2 and NO from the Atmospheric Chemistry Experiment (ACE), Atmos. Chem. Phys. Discuss., 8, 3027–3142, 2008, http://www.atmos-chem-phys-discuss.net/8/3027/2008/.

Kleinböhl, A., Bremer, H., Küllmann, H., Kuttippurath, J., Browell, E. V., Canty, T., Salawitch, R. J., Toon, G. C., and Notholt, J.: Denitrification in the Arctic mid-winter 2004/2005 observed by airborne submillimeter radiometry, Geophys. Res. Lett., 32, L19811, doi:10.1029/2005GL023408, 2005.

Koelemeijer, R. B. A., de Haan, J. F., and Stammes, P.: A database of spectral surface reflectivity in the range 335–772 nm derived from 5.5 years of GOME observations, J. Geophys. Res., 108(D2), 4070, doi:10.1029/2002JD002429, 2003.

Krecl, P., Haley, C. S., Stegman, J., Brohede, S. M., and Berthet, G.: Retrieving the vertical distribution of stratospheric OClO from Odin/OSIRIS limb-scattered sunlight measurements, Atmos. Chem. Phys., 6, 1879–1894, 2006, http://www.atmos-chem-phys.net/6/1879/2006/.

Lambert, A., Read, W., Livesey, N., Santee, M., Manney, G., Froidevaux, L., Wu, D., Schwartz, M., Pumphrey, H., Jimenez, C., Nedoluha, G., Coeld, R., Cuddy, D., Daffer, W., Drouin, B., Fuller, R., Jarnot, R., Knosp, B., Pickett, H., Perun, V., Snyder,

W., Stek, P., Thurstans, R., Wagner, P., Waters, J., Jucks, K., Toon, G., Stachnik, R., Bernath, P., Boone, C., Walker, K., Urban, J., Murtagh, D., Elkins, J., and Atlas, E.: Validation of the Aura Microwave Limb Sounder middle atmosphere water vapor and nitrous oxide measurements, J. Geophys. Res., 112, D24S36, doi:10.1029/2007JD008724, 2007.

Lefèvre, F., Brasseur, G. P., Folkins, I., Smith, A. K., and Simon, P.: Chemistry of the 1991–1992 stratospheric winter: Three-dimensional model simulations, J. Geophys. Res., 99, 8183–8195, 1994.

Lefèvre, F., Figarol, F., Carslaw, K. S., and Peter, T.: The 1997 Arctic ozone depletion quantified from three-dimensional model simulations, Geophys. Res. Lett., 25, 2425–2428, 1998.

Liley, J. B., Johnston, P. V., McKenzie, R. L., Thomas, A. J., and Boyd, I. S.: Stratospheric NO_2 variations from long time series at Lauder, New Zealand, J. Geophys. Res., 105(D9), 11 633–11 640, doi:10.1029/1999JD901157, 2000.

Llewellyn, E. J., Lloyd, N. D., Degenstein, D. A., Gattinger, R. L., Petelina, S. V., Bourassa, A. E., Wiensz, J. T., Ivanov, E. V., McDade, I. C., Solheim, B. H., McConnell, J. C., Haley, C. S., von Savigny, C., Sioris, C. E., McLinden, C. A., Evans, W. F. J., Puckrin, E., Strong, K., Wehrle, V., Hum, R. H., Kendall, D. J. W., Matsushita, J., Murtagh, D. P., Brohede, S., Stegman, J., Witt, G., Barnes, G., Payne, W. F., Piché, L., Smith, K., Warshaw, G., Deslauniers, D. L., Marchand, P., Richardson, E. H., King, R. A., Wever, I., McCreath, W., Kyrölä, E., Oikarinen, L., Leppelmeier, G. W., Auvinen, H., Mégie, G., Hauchecorne, A., Lefévre, F., de La Noë, J., Ricaud, P., Frisk, U., Sjoberg, F., von Schéele, F., and Nordh, L.: The OSIRIS Instrument on the Odin Spacecraft, Can. J. Phys., 82, 411–422, 2004.

Manney, G. L., Krüger, K., Sabutis, J. L., Sena, S. A., and Pawson, S.: The remarkable 2003–2004 winter and other recent warm winters in the Arctic stratosphere since the late 1990s, J. Geophys. Res., 110, D04107, doi:10.1029/2004JD005367, 2005.

Mengistu Tsidu, G., Stiller, G. P., von Clarmann, T., Funke, B., Höpfner, M., Fischer, H., Glatthor, N., Grabowski, U., Kellmann, S., Kiefen, M., Linden, A., López-Puertas, M., Milz, M., Steck, T., and Wang, D. Y.: NO_y from Michelson Interferometer for Passive Atmospheric Sounding on Environmental Satellite during the Southern Hemisphere polar vortex split in September/October 2002, J. Geophys. Res., 110, D11301, doi:10.1029/2004JD005322, 2005.

McLinden, C. A., Olsen, S., Hannegan, B., Wild, O., Prather, M. J., and Sundet, J.: Stratospheric ozone in 3-D models: A simple chemistry and the cross-tropopause flux, J. Geophys. Res., 105(D11), 14 653–14 665, 2000.

McLinden, C. A., Olsen, S., Prather, M. J., and Liley, J. B.: Understanding trends in stratospheric NO_y and NO_2, J. Geophys. Res., 106(D21), 27 787–27 793, 2001.

Murtagh, D., Frisk, U., Merino, F., Ridal, M., Jonsson, A., Stegman, J., Witt, G., Eriksson, P., Jiménez, C., Megie, G., de La Noë, J., Ricaud, P., Baron, P., Pardo, J. R., Hauchcorne, A., Llewellyn, E. J., Degenstein, D. A., Gattinger, R. L., Lloyd, N. D., Evans, W. F. J., McDade, I. C., Haley, C., Sioris, C., von Savigny, C., Solheim, B. H., McConnell, J. C., Strong, K., Richardson, E. H., Leppelmeier, G. W., Kyrölä, E., Auvinen, H., and Oikarinen, L.: An overview of the Odin atmospheric mission, Can. J. Phys., 80, 309–319, 2002.

Nevison, C. D., Solomon, S., and Garcia, R. R.: Model overestimates of NO_y in the upper stratosphere, Geophys. Res. Lett., 24(7), 803–806, doi:10.1029/97GL00549, 1997.

Olsen, S., McLinden, C. A., and Prather, M. J.: Stratospheric N_2O-NO_y system: Testing uncertainties in a 3-D framework, J. Geophys. Res., 106, 28 771–28 784, 2001.

Orsolini, Y., Manney, G., Santee, M., and Randall, C.: An upper stratospheric layer of enhanced HNO_3 following exceptional solar storms, Geophys. Res. Lett., 32, L12S01, doi:10.1029/2004GL021588, 2005.

Osterman, G. B., Sen, B., Toon, G. C., Salawitch, R. J., Margitan, J. J., Blavier, J.-F., Fahey, D. W., and Gao, R. S.: Partitioning of NO_y species in the summer Arctic stratosphere, Geophys. Res. Lett., 26(8), 1157–1160, 1999.

Platt, U.: Differential Optical Absorption Spectroscopy (DOAS), in: Air monitoring by Spectroscopic Techiques, edited by: Sigrist, M., John Wiley & Sons, Inc., 27–84, 1994.

Prather, M. J.: Catastrophic loss of stratospheric ozone in dense volcanic clouds, J. Geophys. Res., 97(D9), 10 187–10 191, 1992.

Qin, G.: Odd nitrogen observations by ACE-FTS, Master's thesis, York University, Toronto, 2007.

Randall, C. E., Harvey, V. L., Manney, G. L., Orsolini, Y., Codrescu, M., Sioris, C., Brohede, S., Haley, C. S., Gordley, L. L., Zawodny, J. M., and Russel III, J. M.: Stratospheric effects of energetic particle precipitation in 2003–2004, Geophys. Res. Lett., 32, L05802, doi:10.1029/2004GL022003, 2005.

Randall, C. E., Harvey, V. L., Singleton, C. S., Bailey, S. M., Bernath, P. F., Codrescu, M., Nakajima, H., and Russel III, J. M.: Energetic particle precipitation effects on the Southern Hemisphere stratosphere in 1992–2005, J. Geophys. Res., 112, D08308, doi:10.1029/2006JD007696, 2007.

Ricaud, P., Lefévre, F., Berthet, G., Murtagh, D., Llewellyn, E. J., Mégie, G., Kyrölä, E., Leppelmeier, W., Auvinen, H., Boone, C., Brohede, S., Degenstein, D. A., de La Noë, J., Dupuy, E., El Amraoui, L., Eriksson, P., Evans, W. F. J., Frisk, U., Gattinger, R. L., Girod, F., Haley, C. S., Hassinen, S., Hauchecorne, A., Jiménez, C., Kyrö, E., Lautié, N., Le Flochmoën, E., Lloyd, N. D., McConnell, J. C., McDade, I. C., Nordh, L., Olberg, M., Petelina, S. V., Sandqvist, A., Seppälä, A., Sioris, C. E., Solheim, B. H., Stegman, J., Strong, K., Taalas, P., Urban, J., von Savigny, C., von Scheele, F., and Witt, G.: Polar vortex evolution during the 2002 Antarctic major warming as observed by the Odin satellite, J. Geophys. Res., 110, D05302, doi:10.1029/2004JD005018, 2005.

Rolph, G. D.: Real-time Environmental Applications and Display sYstem (READY), NOAA Air Resources Laboratory, Silver Spring, MD, http://www.arl.noaa.gov/ready/hysplit4.html(last access: May 2008), 2003.

Roth, C. Z., Degenstein, D. A., Bourassa, A. E., and Llewellyn, E. J.: The retrieval of vertical profiles of the ozone number density using Chappuis band absorption information and a multiplicative algebraic reconstruction technique, Can. J. Phys., 85(11), 1225–1243, doi:10.1139/P07-130, 2007.

Russell III, J. M., Farmer, C. B., Rinsland, C. P., Zander, R., Froidevaux, L., Toon, G. C., Gao, B., Shaw, J., and Gunsen, M.: Measurements of odd nitrogen compounds in the stratosphere by the ATMOS experiment on Spacelab 3, J. Geophys. Res., 93(D2), 1718–1736, doi:10.1029/88JD01604, 1988.

Santee, M., Lambert, A., Read, W., Livesey, N., Coeld, R., Cuddy, D., Daffer, W., Drouin, B., Froidevaux, L., Fuller, R., Jarnot, R., Knosp, B., Manney, G., Perun, V., Snyder, W., Stek, P., Thurstans, R., Wagner, P., Waters, J., Muscari, G., de Zafra, R., Dibb, J., Fahey, D., Popp, P., Marcy, T., Jucks, K., Toon, G., Stachnik, R., Bernath, P., Boone, C., Walker, K., Urban, J., and Murtagh, D.: Validation of the Aura Microwave Limb Sounder HNO_3 Measurements, J. Geophys. Res., 112, D24S40, doi:10.1029/2007JD008721 2007.

Sen, B., Toon, G. C., Osterman, G. B., Blavier, J.-F., Margitan, J. J., Salawitch, R. J., and Yue, G. K.: Measurements of reactive nitrogen in the stratosphere, J. Geophys. Res., 103(D3), 2781–2784, doi:10.1029/97JD02468, 1998.

Seppälä, A., Verronen, P. T., , Kyrölä, E., Hassinen, S., Backman, L., Hauchecorne, A., Bertaux, J. L., and Fussen, D.: Solar proton events of October–November 2003: Ozone depletion in the Northern Hemisphere polar winter as seen by GOMOS/Envisat, Geophys. Res. Lett., 31, L19107, doi:10.1029/2004GL021042, 2004.

Seppälä, A., Verronen, P. T., Clilverd, M. A., Randall, C. E., Tamminen, J., Sofieva, V., Backman, L., and Kyrölä, E.: Arctic and Antarctic polar winter NO_x and energetic particle precipitation in 2002–2006, Geophys. Res. Lett., 34, L12810, doi:10.1029/2007GL029733, 2007.

Shepherd, T. G. and Randel, W. J.: Key issues arising from the 2006 WMO/UNEP Ozone Assessment, SPARC Newsletter, July, 9, 20–22, 2007.

Stiller, G. P., Mengistu Tsidu, G., von Clarmann, T., Glatthor, N., Höpfner, M., Kellmann, S., Linden, A., Ruhnke, R., Fischer, H., López-Puertas, M., Funke, B., and Gil-López, S.: An enhanced HNO_3 second maximum in the Antarctic midwinter upper stratosphere 2003, J. Geophys. Res., 110, D20303, doi:10.1029/2005JD006011, 2005.

Strahan, S. E.: Climatologies of lower stratospheric NO_y and O_3 and correlations with N_2O based on in situ observations, J. Geophys. Res., 104(D23), 2195–2208, doi:10.1029/1999JD900775, 1999.

Strong, K., Wolff, M. A., Kerzenmacher, T. E., Walker, K. A., Bernath, P. F., Blumenstock, T., Boone, C., Catoire, V., Coffey, M., De Mazière, M., Demoulin, P., Duchatelet, P., Dupuy, E., Hannigan, J., Höpfner, M., Glatthor, N., Griffith, D. W. T., Jin, J. J., Jones, N., Jucks, K., Kuellmann, H., Kuttippurath, J., Lambert, A., Mahieu, E., McConnell, J. C., Mellqvist, J., Mikuteit, S., Murtagh, D. P., Notholt, J., Piccolo, C., Raspollini, P., Ridolfi, M., Robert, C., Schneider, M., Schrems, O., Semeniuk, K., Senten, C., Stiller, G. P., Strandberg, A., Taylor, J., Tétard, C., Toohey, M., Urban, J., Warneke, T., and Wood, S.: Validation of ACE-FTS N_2O measurements, Atmos. Chem. Phys., 8, 4759–4786, 2008,
http://www.atmos-chem-phys.net/8/4759/2008/.

Toon, G., Sen, B., Blavier, J., Sasano, Y., Yokota, T., Kanzawa, H., Ogawa, T., Suzuki, M., and Shibasaki, K.: Comparison of Improved Limb Atmospheric Spectrometer and MkIV profiles of atmospheric trace gases measured above Alaska in May 1997, J. Geophys. Res., 107(D24), 8211, doi:10.1029/2001JD000640, 2002.

Toon, G. C.: The JPL MkIV Interferometer, Opt. Photonics News, 2, 19–21, 1991.

Urban, J., Lautié, N., Flochmoën, E. L., Jiménez, C., Eriksson, P., de La Noë, J., Dupuy, E., Amraoui, L. E., Frisk, U., Jégou, F., Murtagh, D., Olberg, M., Ricaud, P., Camy-Peyret, C., Dufour, G., Payan, S., Huret, N., Pirre, M., Robinson, A. D., Harris, N. R. P., Bremer, H., Kleinböhl, A., Küllmann, K., Künzi, K., Kuttippurath, J., Ejiri, M. K., Nakajima, H., Sasano, Y., Sugita, T., Yokota, T., Piccolo, C., Raspollini, P., and Ridolfi, M.: Odin/SMR limb observations of stratospheric trace gases: Validation of N_2O, J. Geophys. Res., 110, D09301, doi:10.1029/2004JD005394, 2005a.

Urban, J., Lautié, N., Le Flochmoën, E., Jiménez, C., Eriksson, P., Dupuy, E., El Amraoui, L., Ekström, M., Frisk, U., Murtagh, D., de La Noë, J., Olberg, M., and Ricaud, P.: Odin/SMR Limb Observations of Stratospheric Trace Gases: Level 2 Processing of ClO, N_2O, O_3, and HNO_3., J. Geophys. Res., 110, D14307, doi:10.1029/2004JD005741, 2005b.

Urban, J., Murtagh, D., Lautié, N., Barret, B., Dupuy, E., de La Noë, J., Eriksson, P., Frisk, U., Jones, A., Le Flochmoën, E., Olberg, M., Piccolo, C., Ricaud, P., and Rösevall, J.: Odin/SMR Limb Observations of Trace Gases in the Polar Lower Stratosphere during 2004–2005, in: Proceedings of the ESA First Atmospheric Science Conference, 8–12 May 2006, Frascati, Italy, edited by: Lacoste, H., ESA-SP-628, European Space Agency publications, European Space Agency, ISBN-92-9092-939-1, ISSN-1609-042X, 2006.

Urban, J., Pommier, M., Murtagh, D., Eriksson, P., and Ricaud, P.: Odin/SMR Limb Observations of Nitric Acid in the Stratosphere, in: Proc. ESA Envisat Symposium, 23–27 April 2007, Montreux, Switzerland, edited by: Lacoste, H., ESA-SP-636, European Space Agency publications, European Space Agency, 2007.

Vitt, F. M., Cravens, T. E., and Jackman, C. H.: A two-dimensional model of thermospheric nitric oxide sources and their contributions to the middle atmospheric chemical balance, J. Atmos. Solar-Terr. Phy., 62(8), 653–667, doi:10.1016/S1364-6826(00)00049-3, 2000.

von Savigny, C., Haley, C. S., Sioris, C. E., McDade, I. C., Llewellyn, E. J., Degenstein, D., Evans, W. F. J., Gattinger, R. L., Griffioen, E., Kyrölö, E., Lloyd, N. D., McConnell, J. C., McLinden, C. A., Mégie, G., Murtagh, D. P., Solheim, B., and Strong, K.: Stratospheric ozone profiles retrieved from limb scattered sunlight radiance spectra measured by the OSIRIS instrument on the Odin satellite, Geophys. Res. Lett., 30(14), 1755, doi:10.1029/2002GL016401, 2003.

Wang, D. Y., H¨pfner, M., Mengistu Tsidu, G., Stiller, G. P., von Clarmann, T., Fischer, H., Blumenstock, T., Glatthor, N., Grabowski, U., Hase, F., Kellmann, S., Linden, A., Milz, M., Oelhaf, H., Schneider, M., Steck, T., Wetzel, G., López-Puertas, M., Funke, B., Koukouli, M. E., Nakajima, H., Sugita, T., Irie, H., Urban, J., Murtagh, D., Santee, M. L., Toon, G., Gunson, M. R., Irion, F. W., Boone, C. D., Walker, K., and Bernath, P. F.: Validation of nitric acid retrieved by the IMK-IAA processor from MIPAS/ENVISAT measurements, Atmos. Chem. Phys., 7, 721–738, 2007,
http://www.atmos-chem-phys.net/7/721/2007/.

Wang, D. Y., Höpfner, M., Blom, C. E., Ward, W. E., Fischer, H., Blumenstock, T., Hase, F., Keim, C., Liu, G. Y., Mikuteit, S., Oelhaf, H., Wetzel, G., Cortesi, U., Mencaraglia, F., Bianchini, G., Redaelli, G., Pirre, M., Catoire, V., Huret, N., Vigouroux, C., De Mazière, M., Mahieu, E., Demoulin, P., Wood, S., Smale, D., Jones, N., Nakajima, H., Sugita, T., Urban, J., Murtagh, D., Boone, C. D., Bernath, P. F., Walker, K. A., Kuttippurath, J., Kleinböhl, A., Toon, G., and Piccolo, C.: Validation of MIPAS HNO3 operational data, Atmos. Chem. Phys., 7, 4905–4934, 2007,
http://www.atmos-chem-phys.net/7/4905/2007/.

WMO: Scientific Assessment of Ozone Depletion: 2006, Global Ozone Research and Monitoring Project-Report, 50, 2007.

Wolff, M. A., Kerzenmacher, T., Strong, K., Walker, K. A., Toohey, M., Dupuy, E., Bernath, P. F., Boone, C. D., Brohede, S., Catoire, V., von Clarmann, T., Coffey, M., Daffer, W. H., De Mazière, M., Duchatelet, P., Glatthor, N., Griffith, D. W. T., Hannigan, J., Hase, F., Höpfner, M., Huret, N., Jones, N., Jucks, K., Kagawa, A., Kasai, Y., Kramer, I., Küllmann, H., Kuttippurath, J., Mahieu, E., Manney, G., McElroy, C. T., McLinden, C., Mébarki, Y., Mikuteit, S., Murtagh, D., Piccolo, C., Raspollini, P., Ridolfi, M., Ruhnke, R., Santee, M., Senten, C., Smale, D., Tétard, C., Urban, J., and Wood, S.: Validation of HNO_3, $ClONO_2$, and N_2O_5 from the Atmospheric Chemistry Experiment Fourier Transform Spectrometer (ACE-FTS), Atmos. Chem. Phys., 8, 3529–3562, 2008,
http://www.atmos-chem-phys.net/8/3529/2008/.